LBL-112 c.2

RADIATION LABORATORY

DOCUMENTS SECTION

PHASE-MATCHED THIRD-HARMONIC GENERATION IN CHOLESTERIC LIQUID CRYSTALS

John W. Shelton
(Ph. D. Thesis)

August 1971

AEC Contract No. W-7405-eng-48

TWO-WEEK LOAN COPY

This is a Library Circulating Copy which may be borrowed for two weeks. For a personal retention copy, call Tech. Info. Division, Ext. 5545

LBL-112 c.2

25

DISCLAIMER

This document was prepared as an account of work sponsored by the United States Government. While this document is believed to contain correct information, neither the United States Government nor any agency thereof, nor the Regents of the University of California, nor any of their employees, makes any warranty, express or implied, or assumes any legal responsibility for the accuracy, completeness, or usefulness of any information, apparatus, product, or process disclosed, or represents that its use would not infringe privately owned rights. Reference herein to any specific commercial product, process, or service by its trade name, trademark, manufacturer, or otherwise, does not necessarily constitute or imply its endorsement, recommendation, or favoring by the United States Government or any agency thereof, or the Regents of the University of California. The views and opinions of authors expressed herein do not necessarily state or reflect those of the United States Government or any agency thereof or the Regents of the University of California.

PHASE-MATCHED THIRD-HARMONIC GENERATION
IN CHOLESTERIC LIQUID CRYSTALS

Table of Contents

Abstract v

I. Introduction 1

II. The Medium 4

III. Linear Theory 11

IV. Non-Linear Theory 42

V. Experiments 61

VI. Discussion and Conclusions 92

Acknowledgments 106

References 107

PHASE-MATCHED THIRD-HARMONIC GENERATION
IN CHOLESTERIC LIQUID CRYSTALS

John W. Shelton

Inorganic Materials Research Division, Lawrence Berkeley Laboratory and
Department of Physics; University of California
Berkeley, California

ABSTRACT

Using Oseen's and de Vries's model, we predict theoretically that phase matching of optical third-harmonic generation can be achieved in cholesteric liquid crystals. The prediction is verified by measurements of third-harmonic generation in mixtures of cholesteryl chloride, cholesteryl myristate, cholesteryl nonanoate and cholesteryl oleyl carbonate. Among the various phase-matched conditions for third-harmonic generation, there are many involving the simultaneous presence of optical waves propagating in opposite directions. This is in sharp contrast to most phase-matching situations which involve all waves propagating in the same direction. This difference arises from the periodicity of the cholesteric structure which is tunable throughout the optical-wavelength region.

We show that phase-matched third-harmonic generation in cholesteric media can be used to measure both the width and asymmetry of ultrashort pulses. No phase-matched second-harmonic generation is observed, implying our cholesteric structures have inversion symmetry on the scale of optical wavelengths.

I. INTRODUCTION

Harmonic generation has been studied in a very large number of materials. There are generally two objectives. Firstly, the creation of laser-like (intense, coherent and collimated) sources of radiation at new frequencies provides new tools for linear and non-linear spectroscopy. Secondly, careful measurements of these non-linear interactions provide data for comparison with theory, thus furthering our understanding of the non-linear properties of materials.

The conversion efficiency of energy from the laser frequency to a harmonic depends critically on the relative phase velocities of the waves, and is most efficient if k-vector conservation or phase matching is achieved.[1] In most media phase matching does not occur. For the case of co-linear third-harmonic generation in isotropic media the phase-matching condition is satisfied if the refractive indices at the fundamental and third-harmonic frequencies are equal. This is not true in typical media since ordinary dispersion implies an increase of the refractive index with frequency. One technique to achieve phase matching in isotropic media is to utilize the anomolous dispersion of an impurity material with strong absorbtion between the fundamental and third-harmonic frequencies to compensate the normal dispersion of the host material.[2,3] More commonly experimenters have utilized either the linear or circular birefringence of a medium to compensate the normal dispersion.[4-7]

Recently interest has arisen in harmonic generation in liquid-crystalline materials,[8,9] in part because of their large possible birefringence and hence potential for achieving phase matching. These materials typically consist of large anisotropic organic molecules.

Under appropriate conditions (e.g. of temperature or concentration) they exhibit both fluidity and ordering properties, such as birefringence. Investigations have been made of second- and/or third-harmonic generation in all three of the major liquid-crystal mesomorphic phases--smectic, nematic and cholesteric.[10-13] There is no convincing evidence of any second-harmonic generation in these media, which in itself is important information about their structures, since it implies they are centro-symmetric on the scale of optical wavelengths.[14]

Third-harmonic generation does not have the same symmetry constraints and in fact has been observed in a number of liquid-crystalline materials.[12,13] No concerted attempt was made to achieve phase-matching although it was suggested that the very high optical rotary power (or circular birefringence) of cholesteric materials might be sufficient to compensate the color dispersion and thus achieve phase matching.

In this thesis we investigate the phase-matching ability of cholesteric liquid crystals in detail. Using Oseen's[15] and de Vries's[16] model for the optical properties of the cholesteric structure, we predict the potential existence of fourteen different phase-matched conditions for third-harmonic generation, most of which arise not from the large circular birefringence of the medium but from its periodic structure. The helical structure of the cholesteric Mesophase gives rise to a spacially-periodic dielectric constant. The periodicity can be tuned throughout the optical wavelength region. The effect of this periodicity on electromagnetic waves has much in common with the effect of a periodic potential on electron waves as well as with all other cases with waves in periodic media.[17,18]

In particular, this periodicity makes possible some very unusual

phase-matching conditions. We can divide them generally into three types: The usual case of both fundamental and third harmonic waves propagating in the same direction, cases in which the phase-matched third-harmonic emerges propagating in a direction opposite to that of the fundamental, and cases in which phase-matched third harmonic is generated only when fundamental waves are simultaneously present propagating in opposite directions. The large number of phase-matching conditions and their unusual nature are due in large part to the tunable and large-scale (~ optical wavelengths) periodicity of cholesteric liquid crystals. In essence, a wave propagating in a periodic medium can be expressed in a Bloch-wave form[17,18] with wave vectors k given by $k_o + \frac{2\pi}{S} N$ where N is an integer and S is the period of the medium. If S can be continuously tuned, then the wave vectors k can be adjusted and consequently many phase-matching conditions can be satisfied.

In the following section we briefly describe the salient properties of cholesteric liquid crystalline materials and a simple model of their structure. In Section III the theory of, linear electromagnetic wave propagation in cholesteric media is discussed at same length for in it lie the essentials for understanding the non-linear theory which follows in Section IV. With the non-linear theory we predict the existence of fourteen conditions for phase-matched third-harmonic generation. Our experiments are described and discussed in Sections V and VI.

II. THE MEDIUM

The detailed structure of the liquid crystalline mesophases is currently under intense investigation and is very far from being well understood.[9] However some simple structural models have proved adequate to explain the most prominent optical properties and also, as we shall see, phase-matched harmonic generation.

The constituent molecules of liquid crystalline materials are typically anisotropic (e.g. rod-shaped) organic molecules (Fig. 2-1). In what is called the nematic structure these molecules have long-range orientational order, tending to line up parallel to each other, but the molecules can move fairly freely past each other parallel to their long axes, giving rise, at least in part, to the medium's fluidity. Because of the molecular alignment, the nematic mesophase is birefringent, although in samples thicker than ~ 0.1 mm non-uniformities in the alignment direction can give rise to turbidity thus obscuring the simple birefringence of the small-scale structure.

The cholesteric structure is simply a twisted version of the nematic. Its constituent molecules not only have an oblong or plate-like shape but also have a particular "handedness," i.e., they are not identical to their mirror images. The cholesteric structure they form is the nematic structure twisted about an axis normal to the molecular alignment so as to form a medium with uniform helical symmetry (Fig. 2-2). In planes normal to the helical symmetry axis (z), there is uniform molecular alignment. The direction of this alignment changes regularly as a function of distance along z. In thick samples ($\gtrsim$ 0.1 mm) the orientation of the helical axis may not be uniform throughout the sample; hence Fig. 2-2 represents a

all the molecules and the dielectric response of the medium is therefore uniform, not periodic.

Light propagating parallel to the helical axis encounters a longitudinal periodic refractive index giving rise to strong reflectivity for $\frac{1}{2}(\lambda/\bar{n}) = p/2$ where $\bar{n}$ is a suitable average refractive index of the medium (see next section). This process is analagous to Bragg reflection. The helical symmetry of the birefringence also gives rise to optical activity which can be as great as 10^4's of degrees in a sample 1 mm thick. All of these properties will be discussed in more detail in the next section.

Cholesteric materials are typically rather viscous,[27] resembling heavy oil. They also are usually very turbid, primarily because of non-uniform orientation of the helical axis throughout the sample. Thin samples ($\lesssim$ 0.1 mm thick) between flat glass can be made optically clear, indicating a relatively uniform structure, and in our experience the helical axis is usually oriented normal to the glass surfaces. This may be due to interactions at the interface favoring the appropriate alignment for molecules in the boundary layer which then carries over into the bulk of thin samples. It could also arise from flow of the material parallel to the glass faces during assembly and from stresses after assembly. These could favor alignment of the long axes of the molecules parallel to the flow and hence encourage the helical axis to be perpendicular to the flow.

time-averaged and small-scale structure. As the name would imply, certain derivatives of cholesterol (e.g., cholesteryl chloride) can have this structure (Fig. 2-3). Some α-helix proteins (e.g., poly-γ-benzyl-L-glutamate) also can form this cholesteric structure.[19]

The period or pitch (p) of the helical structure has a range of from ~ 2500 Å to ∞ (untwisted). It is a function of chemical composition and temperature,[8] and electric and magnetic fields.[20-25] Mixtures of cholesteric materials are usually also cholesteric. The actual difference in angular orientation of neighboring molecules along the helical axis is small; for p = 6000 Å and an average molecular diameter of 30Å, this angle is about 0.6 degree.

The optical properties of this structure are those of a twisted birefringent medium. Thin ($\ll$ p) layers normal to the helical axis are birefringent due to the uniform alignment of the anisotropic molecules. But since the alignment direction changes as a function of position along the helical axis, so also do the principle axes describing the birefringence. The resulting optical properties are those of a birefringent medium twisted about one of its principle axes into a medium with helical symmetry. Light propagating perpendicular to the helical axis and polarized perpendicular to the helical axis encounters a transversely periodic refractive index, producing an interference pattern with maxima at angles θ satisfying $\sin\theta = N\lambda/(p/2)$ where N is an integer and $\lambda = 2\pi\,\omega/c$.[26] (The periodicity of the (linear) optical properties is p/2). With this geometry the liquid crystal is like a grating. For light propagating perpendicular to the helical axis but polarized parallel to the axis, there is no diffraction, since then the light is polarized perpendicular to the long axis of

Chapter II Figure Captions

Fig. 2-1. P-azoxyanisole, which is a nematic liquid crystal in the temperature range 116° to 136°C.

Fig. 2-2. Idealized molecular arrangement in a cholesteric liquid crystal. ξ and η are the molecular-alignment axes, which are twisted around the z-axis with a period p, the pitch.

Fig. 2-3. Cholesterol. Cholesterol itself does not have a liquid-crystal phase, but a number of its derivatives do. For instance, cholesteryl nonanoate is liquid crystalline in the temperature range from 77° to 90°C.

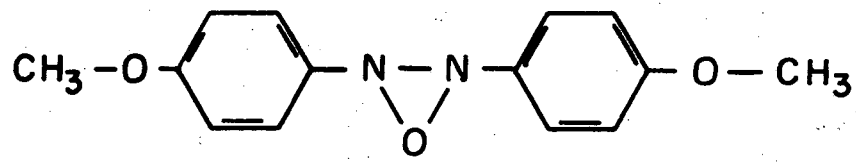

XBL 717-6952

Fig. 2-1

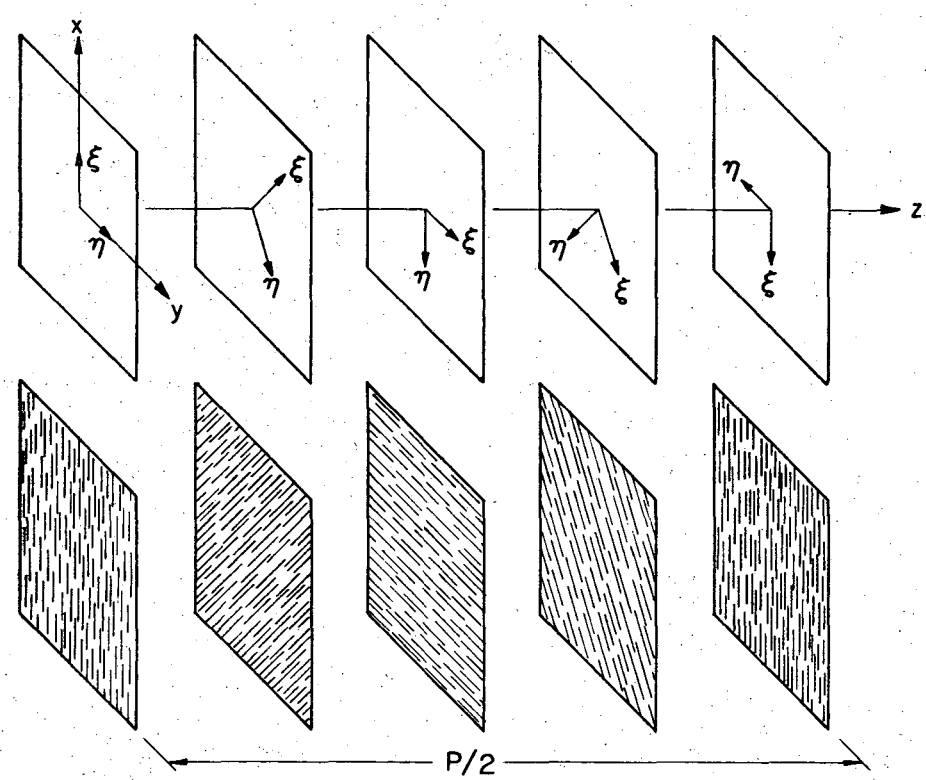

XBL 717-6953

Fig. 2-2

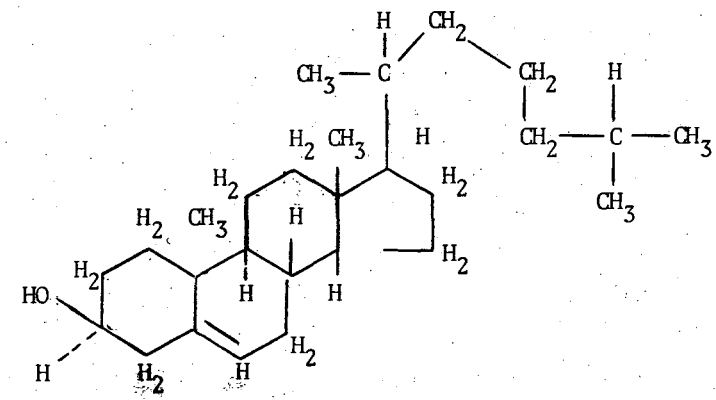

Fig. 2-3

III. LINEAR THEORY

We present in this section a review of relevant linear optical properties of the cholesteric-liquid-crystalline mesophase for light propagating along the direction of helical symmetry. The results are of importance to harmonic generation which will be discussed later. The model was developed by Oseen[15] and de Vries.[16]

It is convenient to introduce two coordinate systems, a cartesian laboratory frame of reference with coordinates x, y and z, and a reference frame with coordinates ξ, η and z, which twists with the cholesteric structure (see Fig. 2-2). The common z-axis is defined to be parallel to the axis of helical symmetry. The components of a vector referred to the laboratory frame (labelled $\mathbf{E}_L$) are related to the same vector's components in the twisted frame (labelled $\mathbf{E}_T$) through a twist transformation having a matrix $\underset{\approx}{T}$:

$$\mathbf{E}_T(\xi, \eta, z) = \underset{\approx}{T}(z)\, \mathbf{E}_L(x, y, z), \tag{3-1}$$

$$\underset{\approx}{T}(z) = \begin{pmatrix} \cos\frac{2\pi}{p}z & \sin\frac{2\pi}{p}z & 0 \\ -\sin\frac{2\pi}{p}z & \cos\frac{2\pi}{p}z & 0 \\ 0 & 0 & 1 \end{pmatrix}. \tag{3-2}$$

p is the pitch or period of the helical structure.

We assume the medium to be characterized by helically-twisted birefringence -- i.e., that sufficiently thin ($\ll$ p) layers normal to the helical axis exhibit simple birefringence with two principle dielectric constants along orthogonal directions specified by the unit

vectors $\hat{\xi}$ and $\hat{\eta}$. These directions twist about the z-axis with period p in the direction $\hat{z}$. Thus the dielectric constant exhibits the helical symmetry and is diagonal in the twisted frame:

$$\underset{\approx}{\varepsilon}_T = \begin{pmatrix} \varepsilon_\xi & 0 & 0 \\ 0 & \varepsilon_\eta & 0 \\ 0 & 0 & \varepsilon_z \end{pmatrix}. \tag{3-3}$$

Without loss of generality it is assumed that $\varepsilon_\eta > \varepsilon_\xi$. The inherent (isotropic liquid phase) optical activity of the molecules is of the order of ~ 0.4 °/mm in our experimental materials. This has a negligible effect on our experiments and thus has been neglected in the theory presented here. For notational simplicity we assume $\underset{\approx}{\varepsilon}$ is real; the effects of absorbtion can easily be added to the final formulae.

For a non-magnetic dielectric medium Maxwell's equations give

$$\begin{aligned} &\nabla \times (\nabla \times \mathbf{E}(\mathbf{r},\omega)) + \frac{\omega^2}{c^2}\, \underset{\approx}{\varepsilon}(\mathbf{r},\omega)\, \mathbf{E}(\mathbf{r},\omega) = 0 \\ &\nabla \cdot (\underset{\approx}{\varepsilon}(\mathbf{r},\omega)\, \mathbf{E}(\mathbf{r},\omega)) = 0 \end{aligned} \tag{3-4}$$

where $\mathbf{E}(\mathbf{r},\omega)$ is the electric field at frequency ω and $\underset{\approx}{\varepsilon}$ is the corresponding dielectric tensor. For waves propagating in the $\pm\hat{z}$ direction in a cholesteric structure, Eq. (3-4) reduces to

$$\left(\frac{\partial^2}{\partial z^2} + \frac{\omega^2}{c^2}\, \underset{\approx}{\varepsilon}_L(z,\omega)\right)\mathbf{E}_L(z,\omega) = 0 \tag{3-5}$$

in the laboratory frame. We have assumed both $\underset{\approx}{\varepsilon}$ and $\mathbf{E}$ have only z spacial dependence. The spacial dependence of $\underset{\approx}{\varepsilon}_L$, which arises from

the twisted birefringence, is eliminated upon transformation into the twisted coordinates (just as the time dependendence of the rotating magnetic field in magnetic resonance is eliminated by a transformation into rotating coordinates). Applying the twist transformation, Eq. (3-2), to Eq. (3-5) gives

$$\left(\frac{\partial^2}{\partial z^2} + \frac{4\pi}{p}\,\underset{\sim}{g}\,\frac{\partial}{\partial z} - \left(\frac{2\pi}{p}\right)^2 + \frac{\omega^2}{c^2}\,\underset{\sim}{\varepsilon}_T(\omega)\right)\underset{\sim}{E}_T(z,\omega) = 0 \tag{3-6}$$

where

$$\underset{\sim}{g} = \begin{pmatrix} 0 & -1 & 0 \\ 1 & 0 & 0 \\ 0 & 0 & 0 \end{pmatrix} . \tag{3-7}$$

The two extra terms in the twisted-frame wave equation are due to the spacial dependence of the transformation.

Solutions to Eq. (3-6) can be determined by assuming[28]

$$\begin{aligned} E_T &= \mathcal{E}\,\hat{e}\,e^{ikz-i\omega t} \\ &\equiv (\mathcal{E}_\xi\,\hat{\xi} + \mathcal{E}_\eta\,\hat{\eta})e^{ikz-i\omega t} , \end{aligned} \tag{3-8}$$

where $\hat{e}$ is a unit polarization vector. This gives

$$\begin{aligned} &\left(-k^2 - \left(\frac{2\pi}{p}\right)^2 + \frac{\omega^2}{c^2}\,\varepsilon_\xi\right)\mathcal{E}_\xi - i\,\frac{4\pi}{p}\,k\,\mathcal{E}_\eta = 0 \\ &+ i\,\frac{4\pi}{p}\,k\,\mathcal{E}_\xi + \left(-k^2 - \left(\frac{2\pi}{p}\right)^2 + \frac{\omega^2}{c^2}\,\varepsilon_\eta\right)\mathcal{E}_\eta = 0 . \end{aligned} \tag{3-9}$$

Non-zero solutions for $\mathcal{E}_\xi$ and $\mathcal{E}_\eta$ exist only when the determinant of their coefficients is zero. The resultant expressions for k and the corresponding polarizations follow:

$$m_1'^2 = 1 + \lambda'^2 - \sqrt{4\lambda'^2 + \alpha^2} \tag{3-10a}$$

$$m_2'^2 = 1 + \lambda'^2 + \sqrt{4\lambda'^2 + \alpha^2} \tag{3-10b}$$

$$\begin{aligned} \left(\frac{\mathcal{E}_\eta}{\mathcal{E}_\xi}\right)_{1,2} &\equiv if_{1,2} = i\left(\frac{\lambda'^2 + m_{1,2}'^2 + \alpha - 1}{2m_{1,2}'\lambda'}\right) \\ &= \frac{-2im_{1,2}'\lambda'}{\lambda'^2 + m_{1,2}'^2 - \alpha - 1} \end{aligned} \tag{3-11}$$

where

$$k_{1,2} \equiv m_{1,2}\,\frac{\omega}{c} \tag{3-12a}$$

$$m_{1,2}' \equiv \frac{m_{1,2}'}{\sqrt{\varepsilon}} \tag{3-12b}$$

and

$$\lambda' \equiv \frac{2\pi\omega}{pc\sqrt{\varepsilon}} \tag{3-13}$$

$$\varepsilon \equiv \frac{1}{2}(\varepsilon_\xi + \varepsilon_\eta) \tag{3-14}$$

$$\alpha \equiv \frac{\varepsilon_\eta - \varepsilon_\xi}{\varepsilon_\xi + \varepsilon_\eta} \geq 0 \tag{3-15}$$

Formally, m_1 and m_2 are the twisted-frame refractive indices, but because of the unusual coordinate system their valves (Fig. 3-1a) bear little resemblance to ordinary refractive indices. Note that the only parameters of the medium which enter these expressions are $\varepsilon_\xi(\omega)$, $\varepsilon_\eta(\omega)$ and p.

The magnetic field $\underset{\sim}{B}$ associated with each solution for the electric field $\underset{\sim}{E}$ can be obtained by transforming the appropriate Maxwell equation into the twisted coordinates:

$$\underset{\approx}{T}: \quad \left(-\frac{1}{c}\frac{\partial}{\partial t}\underset{\sim}{B}_L = \underset{\sim}{\nabla}_L \times \underset{\sim}{E}_L = \underset{\approx}{\sigma}\frac{\partial}{\partial z}\underset{\sim}{E}_L \right)$$

$$-\frac{1}{c}\frac{\partial}{\partial t}\underset{\sim}{B}_T = \underset{\approx}{\sigma}\frac{\partial}{\partial z}\underset{\sim}{E}_T - \frac{2\pi}{p}\underset{\sim}{E}_T \tag{3-16}$$

where again we have assumed $\underset{\sim}{E}$ has only z spacial dependence. Hence, for each solution (or normal mode),

$$\underset{\sim}{B}_T = \begin{pmatrix} i\frac{\lambda}{p} & -m \\ m & i\frac{\lambda}{p} \end{pmatrix} \underset{\sim}{E}_T$$

or (3-17)

$$B_\xi = -\frac{\sqrt{\varepsilon}}{q} E_\eta$$

$$B_\eta = +q\sqrt{\varepsilon}\, E_\xi$$

where

$$q \equiv m' - \lambda' f = \frac{f}{m' f - \lambda'} \tag{3-18}$$

Poynting's vector can then be expressed in terms of the electric field in the twisted-coordinates. The result, for a single mode, is

$$\langle \underset{\sim}{S} \rangle_t = \frac{c\sqrt{\varepsilon}}{8\pi} |\mathcal{E}|^2 \frac{\mathrm{Re}\left(q + \frac{|f|^2}{q}\right)}{1 + |f|^2} \hat{z} \tag{3-19}$$

where Re indicates the real part of its argument.

There are four solutions of the wave equation, corresponding to the four values of m ($\pm m_1$, $\pm m_2$). Two of the waves propagate in the forward ($+\hat{z}$) direction and two in the backward direction. However the direction of the phase velocity (in the twisted frame) is not always the same as the direction of energy flow (Poynting's vector, $\underset{\sim}{S}$). (We are assuming ordinary dispersion, so that the direction of Poynting's vector for a single frequency is the same as the direction of the group velocity.) From Eq. (3-19) it is apparent that the sign of $\underset{\sim}{S}$ is the same as the sign of Re(q) which in turn is related to m. We have adopted the convention of calling modes with positive ($+\hat{z}$) Poynting vectors the <u>forward</u> (propagating) modes, which has the consequence that the sign of k_1 (or m_1) must be negative in the region $\lambda'^2 > 1 + \alpha$ to describe a forward wave (Table 3-1).

Fig. 3-1 shows typical values of the three basic parameters m', f and q for the two forward propagating modes. For $1-\alpha < \lambda'^2 < 1+\alpha$, m'_1, f_1 and q_1 are pure imaginary. In this region around $\lambda' = 1$, cholesteric media exhibit strong reflection of the incident polarization feeding into mode 1 (Fig. 3-6). This reflectivity occurs because the periodic strucutre's linear-optical periodicity, p/2, is just half the reflected wavelength inside the medium:

$$p/2 = \lambda_o/2\sqrt{\varepsilon} \tag{3-20}$$

or

$$\lambda' = \frac{\lambda_o}{p\sqrt{\varepsilon}} = 1 \tag{3-21}$$

where $\lambda_o = 2\pi \frac{\omega}{c}$. A more complete discussion of boundry value conditions and the reflectivity is given later.

From Fig. 3-1 it is apparent that both modes (excluding mode 1 near its reflection band) are in general elliptically polarized in the twisted coordinate system, becoming linearly and circularly polarized in the limits $\lambda' \to 0$ and $\lambda' \to \infty$ respectively. As viewed in the laboratory frame the normal mode polarizations will have a superimposed spacial twist. The general constant-elliptical polarization in the twisted frame appears in the laboratory frame as a twisted-elliptical polarized wave with the same ellipticity as in the twisted frame but with its major axis twisted or rotating at the spacial rate $2\pi/p$ radians per unit length. This may be seen mathematically by transforming the twisted frame solutions back into the lab frame, which yields, for each normal mode

$$\mathcal{E}_L = \frac{\mathcal{E}}{\sqrt{1+|f|^2}} \left((\hat{x} \operatorname{Cos} \frac{2\pi}{p} z + \hat{y} \operatorname{Sin} \frac{2\pi}{p} z) + if(-\hat{x} \operatorname{Sin} \frac{2\pi}{p} z + \hat{y} \operatorname{Cos} \frac{2\pi}{p}) \right) e^{ikz-i\omega t} \tag{3-22}$$

This laboratory-frame expression for each mode may be resolved into a superposition of left and right circularly polarized components, each with different amplitudes and different propagation constants. For each mode

$$\mathcal{E}_L = \frac{\mathcal{E}}{\sqrt{1+|f|^2}} \left[A^+ \left(\frac{\hat{x} + i\hat{y}}{\sqrt{2}} \right) e^{in^+ \frac{\omega}{c} z - i\omega t} + A^- \left(\frac{\hat{x} - i\hat{y}}{\sqrt{2}} \right) e^{in^- \frac{\omega}{c} z - i\omega t} \right] \tag{3-23}$$

where

$$A^\pm = \frac{1 \pm f}{\sqrt{2}} \tag{3-24}$$

and

$$n^\pm = m \mp \frac{\lambda_o}{p} \quad . \tag{3-25}$$

Two of the four effective refractive indices $\left(n^\pm_{1,2}\right)$ in this representation have unusual values (Fig. 3-2), differing significantly from $\sqrt{\varepsilon}$, the average index of the medium. The corresponding amplitudes of these wave components are small (Fig. 3-3) but essential in many of the phase-matched third-harmonic generation conditions to be derived.

Clearly the detailed character of the solutions is strongly dependent on the ratio of wavelength to pitch. In the limit of $\lambda' \to 0$ (or $p \to \infty$) the medium is untwisted and the normal modes are linearly polarized along the two principle axes, as occurs in ordinary (untwisted) birefringent media. In the opposite limit of $\lambda' \to \infty$ ($p \to 0$) the helical character of the structure is on an infinitessimal scale compared to a wavelength and the normal modes become circularly polarized in opposite senses as in optically active media. Between these two limits the normal modes are generally intermediate in character. For very small but finite λ' ($0 < \lambda' \lesssim \frac{1}{3}\alpha$) the modes are nearly linearly polarized along $\hat{\xi}$ and $\hat{\eta}$ in the twisted frame and hence appear as twisted (or rotating in space) linear polarizations in the laboratory frame with a spacial twist rate equal to that of the cholesteric structure, namely $2\pi/p$ radians per unit length. If both modes are excited, the overall behaviour is more complicated because the two modes have different propagation constants.

For $\alpha \lesssim \lambda' \lesssim 1 - \alpha$ and $\lambda' > 1 + \alpha$ both normal modes are approximately circularly polarized in the laboratory frame. The relative amplitude (Eq. 3-24) of the stronger pure circularly-polarized component of each mode is greater than 3. Hence the medium exhibits approximate optical activity (approximate in the sense that incident linearly polarized light emerges not as purely linearly polarized but always slightly elliptically polarized[15]). For a right-handed cholesteric material, the dominant laboratory-frame circularly polarized components are A_1^- and A_2^+. Thus the approximate optical activity is given by

$$R\left(\frac{\text{radians}}{\text{unit length}}\right) = \frac{1}{2}\frac{\omega}{c}(n_1^- - n_2^+) \tag{3-26}$$

$$= \frac{\pi}{\lambda_o}\left(m_1 - m_2 + 2\frac{\lambda_o}{p}\right) \tag{3-27}$$

$$\simeq \frac{-\pi\alpha^2}{4p\lambda'^2(1-\lambda'^2)} \quad . \tag{3-28}$$

Fig. 3-4 illustrates the dependence of the optical activity on λ'. Note that although Eq. (3-28) is singular at $\lambda' = 1$ and 0, the optical activity is not infinite; both the conceptual and mathematical approximations used in deriving Eqs. (3-26) and (3-28) respectively are invalid near $\lambda' = 1$ and 0.

The reflectivity of a cholesteric medium is obtained through consideration of the boundry conditions. Suppose a planer monochromatic wave in an isotropic medium of refractive index n_o is normally incident on a semi-infinite slab of cholesteric material with its helical axis normal to the interface. The incident, reflected and transmitted fields are written as follows:

Incident field:

$$\begin{pmatrix} E_x \\ E_y \end{pmatrix} = \begin{pmatrix} e_x \\ e_y \end{pmatrix} e^{in_o\frac{\omega}{c}z - i\omega t}$$

$$\begin{pmatrix} B_x \\ B_y \end{pmatrix} = \begin{pmatrix} -e_y \\ e_x \end{pmatrix} e^{in_o\frac{\omega}{c}z - i\omega t} \tag{3-29}$$

Reflected field:

$$\begin{pmatrix} E'_x \\ E'_y \end{pmatrix} = \begin{pmatrix} e'_x \\ e'_y \end{pmatrix} e^{-in_o\frac{\omega}{c}z - i\omega t}$$

$$\begin{pmatrix} B'_x \\ B'_y \end{pmatrix} = n_o \begin{pmatrix} e'_y \\ -e'_x \end{pmatrix} e^{-in_o\frac{\omega}{c}z - i\omega t} \tag{3-30}$$

Transmitted field:

$$\begin{pmatrix} E_\xi \\ E_\eta \end{pmatrix} = A_1 \begin{pmatrix} 1 \\ if_1 \end{pmatrix} e^{ik_1 z - i\omega t} + A_2 \begin{pmatrix} 1 \\ if_2 \end{pmatrix} e^{ik_2 z - i\omega t}$$

$$\begin{pmatrix} H_\xi \\ H_\eta \end{pmatrix} = \sqrt{\varepsilon}\ A_1 \begin{pmatrix} -i\frac{f_1}{q_1} \\ q_1 \end{pmatrix} e^{ik_1 z - i\omega t} + A_2 \begin{pmatrix} \frac{-if_2}{q_2} \\ q_2 \end{pmatrix} e^{ik_2 z - i\omega t} . \tag{3-31}$$

With the boundary at $z = 0$ (where $\hat{\xi} = \hat{x}$ and $\hat{\eta} = \hat{y}$) continuity of tangential $\underset{\sim}{E}$ and $\underset{\sim}{H}$ $(=\underset{\sim}{B})$ implies

$$\begin{aligned} e_x + e'_x &= A_1 + A_2 \\ e_y + e'_y &= i(f_1 A_1 + f_2 A_2) \\ e_y - e'_y &= i\tilde{n}\left(\frac{f_1}{q_1} A_1 + \frac{f_2}{q_2} A_2\right) \\ e_x - e'_x &= \tilde{n}\,(q_1 A_1 + q_2 A_2) \end{aligned} \tag{3-32}$$

where $\tilde{n} = \frac{\sqrt{\varepsilon}}{n_o}$.

Consequently we obtain

$$\begin{aligned} 2e_x &= (1 + \tilde{n}q_1)\, A_1 + (1 + \tilde{n}q_2)\, A_2 \\ -2ie_y &= f_1\left(1 + \frac{\tilde{n}}{q_1}\right) A_1 + f_2\left(1 + \frac{\tilde{n}}{q_2}\right) A_2 \end{aligned} \tag{3-33}$$

$$\begin{aligned} A_1 &= D^{-1}\ f_2\left(1 + \frac{\tilde{n}}{q_2}\right) e_x + i(1 + \tilde{n}q_2)\, e_y \\ A_2 &= D^{-1}\ -f_1\left(1 + \frac{\tilde{n}}{q_1}\right) e_x - i(1 + \tilde{n}q_1)\, e_y \end{aligned} \tag{3-34}$$

$$\begin{aligned} e'_x &= A_1 + A_2 - e_x \\ e'_y &= if_1 A_1 + if_2 A_2 - e_y , \end{aligned} \tag{3-35}$$

where

$$D \equiv \frac{1}{2}\ (1 + \tilde{n}q_1)\, f_2\, \left(1 + \frac{\tilde{n}}{q_2}\right) - (1 + \tilde{n}q_2)\, f_1\, \left(1 + \frac{\tilde{n}}{q_1}\right) \tag{3-36}$$

From Eq. (3-33) one can calculate the incident polarizations which feed exclusively into each of the normal modes. These polarizations differ significantly from the two circular polarizations only near $\lambda' = 0$. The sense or handedness of the incident polarization[29] which feeds into mode 1 is the same as the handedness of the cholesteric structure. The reflectivity of the cholesteric medium for these same two incident polarizations is shown in Fig. 3-6. The reflectivity of sufficiently thick (typically $\gtrsim 50$ p) samples is independent of the thickness,[16] due to the finite penetration depth of the reflected wave. For essentially the same reason, the band of total reflectivity (of mode 1) has finite width.

In ordinary (untwisted) birefringent media, the polarizations ($\propto \underset{\sim}{E}$) of the two normal modes corresponding to each given propagation direction are orthogonal. In a cholesteric structure (for light propagating along the twist axis) this is not true. Since transverse (in xy plane) scalar products are invariant under the twist transformation one can express such quantities directly in terms of the fields of the twisted frame. Thus

$$\hat{e}_1^{\,\dagger} \cdot \hat{e}_2 = \frac{1 + f_1^{\,*} f_2}{\sqrt{1 + |f_1|^2}\ \sqrt{1 + f_2^{\,2}}} \tag{3-37}$$

This expression is non-zero except in the two limiting cases $\alpha \to 0$ and $\lambda' \to \infty$.

Although one might expect the lack of orthogonality to lead to cross terms in the expression for Poynting's vector when both modes are excited, this is not the case. In the general expression for Poynting's vector outside the reflection band,

$$\langle \underset{\sim}{S} \rangle_t = \frac{c\sqrt{\varepsilon}}{8\pi} \left[\mathcal{E}_1^{\,2} \left(\frac{q_1 + \frac{f_1^{\,2}}{q_1}}{1 + f_1^{\,2}} \right) + \mathcal{E}_2^{\,2} \left(\frac{q_2 + \frac{f_2^{\,2}}{q_2}}{1 + f_2^{\,2}} \right) \right.$$

$$\left. + \frac{\mathcal{E}_1 \mathcal{E}_2}{\sqrt{1 + f_1^2}\ \sqrt{1 + f_2^2}} \quad (q_1 + q_2)\left(1 + \frac{f_1 f_2}{q_1 q_2}\right) \quad \mathrm{Cos}(k_1 - k_2)z \right] \hat{z}, \qquad (3\text{-}38)$$

the quantitity $\left(1 + \frac{f_1 f_2}{q_1 q_2}\right)$ is identically zero. However it will be pointed out later that the lack of orthogonality <u>can</u> be relevant in non-linear interactions.

The propagation of electromagnetic waves along the helical axis in a cholesteric medium has many characteristics in common with the propagation of electrons in a one-dimensional periodic lattice. Both situations, as well as a host of others, are described by waves interacting with a periodic medium. Bloch's theorm[17,18] is generally applicable to such problems, and we shall rederive here the polarizations and dispersion relations of the normal modes using this theorm.

In a cholesteric structure, which has a periodic dielectric susceptibility, solutions for the electric field can be expressed in the form

$$\underset{\sim}{E} = e^{i\kappa z}\, \underset{\sim}{u}(\kappa, z)\, e^{-i\omega t} \qquad (3\text{-}39)$$

where $\underset{\sim}{u}(\kappa,z)$ has the periodicity of the susceptibility which is p/2 for linear-optical phenomena. Substitution into the wave equation (Eq. (3-4)) gives the equation for $\underset{\sim}{u}$:

$$\left(\frac{\partial^2}{\partial z^2} + 2i\kappa \frac{\partial}{\partial z} - \kappa^2 + \frac{\omega^2}{c^2} \underset{\approx}{\varepsilon}(z) \right) \underset{\sim}{u}(\kappa, z) = 0 \qquad (3\text{-}40)$$

Since both $\underset{\approx}{\varepsilon}(z)$ and $\underset{\sim}{u}(\kappa,z)$ have the periodicity p/2 they both may be expanded in series containing only "reciprocal-lattice-vector" components:

$$\underset{\sim}{u}(\kappa, z) = \sum_G C_G(\kappa) e^{iGz} \qquad (3\text{-}41)$$

$$\underset{\approx}{\varepsilon}(z) = \sum_G \underset{\approx}{\varepsilon}_G\, e^{iGz} \quad , \qquad (3\text{-}42)$$

where $G = N \frac{4\pi}{p}$ with N being any integer. Substituting and taking the scalar product with e^{igz} yields

$$(\kappa + g)^2 \underset{\sim}{C}_g - \frac{\omega^2}{c^2} \sum_G \underset{\approx}{\varepsilon}_G \underset{\sim}{C}_{g-G} = 0 \qquad (3\text{-}43)$$

Typically, the potential of a lattice for an electron contains many (perhaps ∞) Fourier components. In a cholesteric structure the dielectric constant has only three (complex) Fourier components, which contributes to making exact solutions obtainable. In the laboratory frame

$$\underset{\approx}{\varepsilon}(x,y) = \varepsilon \left[\underset{\approx}{I} + \alpha \begin{pmatrix} \cos \frac{4\pi}{p} z & \sin \frac{4\pi}{p} z \\ \sin \frac{4\pi}{p} z & -\cos \frac{4\pi}{p} z \end{pmatrix} \right] \tag{3-44}$$

where $\underset{\approx}{I}$ is the unit matrix, and $\varepsilon = \frac{1}{2}(\varepsilon_\xi + \varepsilon_\eta)$ and $\alpha = \frac{\varepsilon_\eta - \varepsilon_\xi}{\varepsilon_\xi + \varepsilon_\eta}$ as before. Because of the helical symmetry of the cholesteric structure, we gain formal simplicity by working in circularly polarized transverse coordinates ($\hat{+} \equiv \frac{\hat{x} + i\hat{y}}{\sqrt{2}}$, $\hat{-} \equiv \frac{\hat{x} - i\hat{y}}{\sqrt{2}}$, z).

Thus we obtain

$$\underset{\approx}{\varepsilon}(+,-) = \varepsilon \begin{pmatrix} 1 & \alpha e^{-i\frac{4\pi}{p}z} \\ \alpha e^{+i\frac{4\pi}{p}z} & 1 \end{pmatrix}. \tag{3-45}$$

This tensor has only 0 and $\pm \frac{4\pi}{p}$ complex Fourier components.

From Eq. (3-43) one then obtains an infinite set of scalar equations (two for each value of g taken from the reciprocal lattice vectors) in the infinite number of unknowns $C_g^{\pm}$ (resolving the vector $\underset{\approx}{C}_g$ into its $\hat{+}$ and $\hat{-}$ components):

$$\begin{array}{ccccc}
 & \vdots & & \vdots & \\
(\kappa + 2Q)^2 - \varepsilon \frac{\omega^2}{c^2} & C_{2Q}^- & & - \alpha\varepsilon \frac{\omega^2}{c^2} & C_Q^+ = 0 \\
 & - \alpha \frac{\omega^2}{c^2} & C_{2Q}^- & + (\kappa + Q)^2 - \varepsilon \frac{\omega^2}{c^2} & C_Q^+ = 0 \\
(\kappa + Q)^2 - \varepsilon \frac{\omega^2}{c^2} & C_Q^- & & - \alpha\varepsilon \frac{\omega^2}{c^2} & C_o^+ = 0 \\
 & - \alpha\varepsilon \frac{\omega^2}{c^2} & C_Q^- & + \kappa^2 - \varepsilon \frac{\omega^2}{c^2} & C_o^+ = 0 \\
\kappa^2 - \varepsilon \frac{\omega^2}{c^2} & C_o^- & & - \alpha\varepsilon \frac{\omega^2}{c^2} & C_{-Q}^+ = 0 \\
 & - \alpha\varepsilon \frac{\omega^2}{c^2} & C_o^- & + (\kappa - Q)^2 + \varepsilon \frac{\omega^2}{c^2} & C_{-Q}^+ = 0 \\
 & \vdots & & \vdots &
\end{array} \tag{3-46}$$

where $Q = \frac{4\pi}{p}$. In matrix form,

$$
\begin{bmatrix}
\cdots & {}^{+}C_{2Q} & {}^{-}C_{2Q} & {}^{+}C_{Q} & {}^{-}C_{Q} & {}^{+}C_{0} & {}^{-}C_{0} & {}^{+}C_{-Q} & \cdots
\end{bmatrix}
=
\begin{bmatrix}
\cdots & 0 & 0 & 0 & 0 & 0 & 0 & 0 & \cdots \\
\cdots & 0 & 0 & 0 & 0 & 0 & 0 & 0 & \cdots \\
\cdots & 0 & 0 & 0 & 0 & 0 & 0 & 0 & \cdots \\
\cdots & 0 & 0 & 0 & 0 & 0 & 0 & 0 & \cdots \\
\cdots & 0 & 0 & 0 & 0 & 0 & 0 & 0 & \cdots \\
\cdots & 0 & 0 & 0 & 0 & 0 & 0 & 0 & \cdots \\
\cdots & 0 & 0 & 0 & 0 & 0 & 0 & 0 & \cdots \\
\cdots & 0 & 0 & 0 & 0 & 0 & 0 & 0 & \cdots
\end{bmatrix}
\times
\begin{bmatrix}
(\kappa+2Q)^2-\varepsilon & \frac{2}{3}|^2_c & 0 & 0 & 0 & 0 & 0 & 0 & \cdots \\
\frac{2}{3}|^2_c & (\kappa+2Q)-\varepsilon & \frac{2}{3}|^2_c & -\alpha\varepsilon & 0 & 0 & 0 & 0 & \cdots \\
0 & \frac{2}{3}|^2_c & (\kappa+Q)^2-\varepsilon & \frac{2}{3}|^2_c & 0 & 0 & 0 & 0 & \cdots \\
0 & -\alpha\varepsilon & \frac{2}{3}|^2_c & (\kappa+Q)^2-\varepsilon & \frac{2}{3}|^2_c & -\alpha\varepsilon & 0 & 0 & \cdots \\
0 & 0 & 0 & \frac{2}{3}|^2_c & \kappa^2-\varepsilon & \frac{2}{3}|^2_c & 0 & 0 & \cdots \\
0 & 0 & 0 & -\alpha\varepsilon & \frac{2}{3}|^2_c & \kappa^2-\varepsilon & -\alpha\varepsilon & \frac{2}{3}|^2_c & \cdots \\
0 & 0 & 0 & 0 & 0 & \frac{2}{3}|^2_c & (\kappa-Q)^2-\varepsilon & \frac{2}{3}|^2_c & \cdots \\
\vdots & \vdots & \vdots & \vdots & \vdots & \vdots & \vdots & \vdots & \ddots
\end{bmatrix}
\tag{3-47}
$$

Non-zero solutions for the amplitudes $C_G^{\pm}$ exist when the determinant of the coefficient matrix vanishes. The form of the matrix allows the determinant to be expressed as a product of the determinants of the smaller 2×2 matricies along the diagonal. All of these smaller matrices are identical except by translations in k-space by reciprocal lattice vectors. This is a consequence of κ in Eq. (3-39) being defined only modulo $4\pi/p$. It is sufficient to solve only one of the 2×2 matrices. Solving for example the matrix determining the amplitudes C_Q^- and C_Q^+ yields for the allowed values of ε

$$
\left(\kappa + \frac{2\pi}{p}\right)^2 = \varepsilon \frac{\omega^2}{c^2} \, 1\left(+ \lambda'^2 \pm \sqrt{4\lambda'^2 + \alpha^2}\right) \tag{3-48}
$$

using again the paramaterization of Eqs. (3-12) - (3-15). Comparison with Eqs. (3-10) and (3-12) shows that

$$
\kappa = k_T - \frac{2\pi}{p} , \tag{3-49}
$$

where k_T is any of the twisted-frame propagation constants discussed previously (Eqs. (3-10) and (3-12)). The corresponding solution for the electric field, expressed in Bloch form, is

$$
\underset{\sim}{E} = e^{i\left(k_T - \frac{2\pi}{p}\right) z} \times
$$

$$
\frac{\mathcal{E}_\xi}{2}\left((1+f)(\hat{x}+i\hat{y}) + (1-f)(\hat{x}-i\hat{y})\, e^{i\frac{4\pi}{p} z}\right) e^{i\omega t} \tag{3-50}
$$

where $\mathcal{E}_\xi$ is an arbitrary amplitude and f is given by Eq. (3-11). The actual solution for the electric field obtained by first solving any of the other 2 × 2 matrices in Eq. (3-47) is identical to Eq. (3-50). This same expression can be obtained immediately from the laboratory-frame resolution of each mode into its circularly polarized components, Eq. (3-23).

The reflection band of mode 1 in cholesteric structures is analogous to the band gaps of electrons in lattices. However in contrast to the electron case, in a cholesteric structure there is only one gap (for propagation parallel to the helical axis)[30] and for only one of the two normal mode polarizations. There are three related sources of this difference: the two-dimensionality of the electron magnetic wave equation, the "handedness" symmetry of the cholesteric structure, and the small number of Fourier components of the periodic dielectric response. The situation has some similarity to a diffraction grating with a sinusoidally varying transmission characteristic in the plane of the grating; such a grating has only zeroth- and first-order interference maxima, which is formally related to the fact that the Fourier transform of its transmission pattern has only three complex Fourier components. Similarly, a cholesteric liquid crystal has a sinusoidally varying dielectric constant (as a function of z) giving rise to only three complex Fourier components. However this fact alone is insufficient to explain the single band gap in cholesteric liquid crystals, since and electron in a one-dimensional sinusoilal potential would still have higher order gaps. The additional critical differences are the helical symmetry of the cholesteric

structure and the higher spacial dimensionality of the wave equation. Note that the solutions derived in this section are exact; unlike the electron case, each solution consists of a superposition of just two plane harmonic waves (Eq. (3-23).

Direction of Poynting's vector	Expression for m'		
	Mode 1		Mode 2
	$\lambda'^2 < 1-\alpha$	$\lambda'^2 > 1+\alpha$	All λ'
$+\hat{z}$	$+\sqrt{1+\lambda'^2-\sqrt{4\lambda'^2+\alpha^2}}$	$-\sqrt{1+\lambda'^2-\sqrt{4\lambda'^2+\alpha^2}}$	$+\sqrt{1+\lambda'^2+\sqrt{4\lambda'^2+\alpha^2}}$
$-\hat{z}$	$-\sqrt{1+\lambda'^2-\sqrt{4\lambda'^2+\alpha^2}}$	$+\sqrt{1+\lambda'^2-\sqrt{4\lambda'^2+\alpha^2}}$	$-\sqrt{1+\lambda'^2+\sqrt{4\lambda'^2+\alpha^2}}$

Table 3-1. The expressions for m' corresponding to the two directions ($\pm\hat{z}$) of Poynting's vector for each normal mode.

Chapter III Figure Captions

Fig. 3-1. The values of m', f and q for the two forward modes (Poynting vector in + $\hat{z}$ direction) in a right-handed cholesteric structure ($p > 0$) with $\alpha = 0.03$, as a function of $\lambda'(=\frac{\lambda_o}{p\sqrt{\varepsilon}}$, where $\lambda_o = 2\pi\frac{\omega}{c}$). For $1-\alpha < \lambda'^2 < 1+\alpha$, m_1', f_1 and q_1 are pure imaginary; their values, divided by $\sqrt{-1}$, are plotted as dashed lines. For the backward propagating modes all signs change. For a left-handed helical structure ($p < 0$), the signs of f_1 and f_2 change.

Fig. 3-2. Normalized refractive indices for the two circularly polarized components of each forward normal mode in the laboratory frame for $\alpha = 0.03$ and a right-handed cholesteric structure. n_1^- and n_2^+ are actually not equal, but are virtually indistinguishable on the scale of this graph. In the reflection band (around $\lambda' = 1$, both n_1^+ and n_1^- are pure imaginary. For a left-handed structure the senses ("+" and "-") are reversed. For the backward propagating modes, the senses are reversed and all signs change.

Fig. 3-3. The relative amplitudes of the two circularly polarized components of each forward normal mode in the laboratory frame, for $\alpha = 0.03$ and a right-handed cholesteric structure. For a left-handed structure the ratio for each mode is inverted. For the backward propagating modes, the ratio for each mode is inverted. (The handedness's of the backward-mode polarizations with respect to their backward propagation direction are however unchanged.)

Fig. 3-4. Optical rotation in a cholesteric material with $\alpha = 0.03$ and $\sqrt{\varepsilon} = 1.5$ for light propagating along the helical axis. For $\lambda' > 1$ the sense of rotation is the same as the sense of the cholesteric structure; for $\lambda' < 1$ these senses are opposite. The curve is a

plot of Eq. (3-27) outside of the reflection band; it is dashed for $\lambda' < \alpha$ and $1 - \alpha < \lambda' < 1 + \alpha$ where optical activity does not approximate the medium's optical properties.

Fig. 3-5. Polarization of normally-incident light which feeds exclusively into each of the two forward normal modes 1 and 2, for $\alpha = 0.03$, $\tilde{n} = 1$, and a semi-infinite slab of right-handed cholesteric material with its helical axis normal to the interface. The upper (lower) curve indicates that except near $\lambda' = 0$ left-(right) circularly polarized light, $\hat{x} + i\hat{y}$ ($\hat{x} - i\hat{y}$) efficiently excites mode 2 (1) in a right-handed cholesteric structure.

Fig. 3-6. Reflectivity of light normally incident on a semi-infinite slab of idealized cholesteric material with its helical axis normal to the interface. The curve R1(R2) is for the incident polarization feeding exclusively into mode 1(2) (see Fig. 3-5).

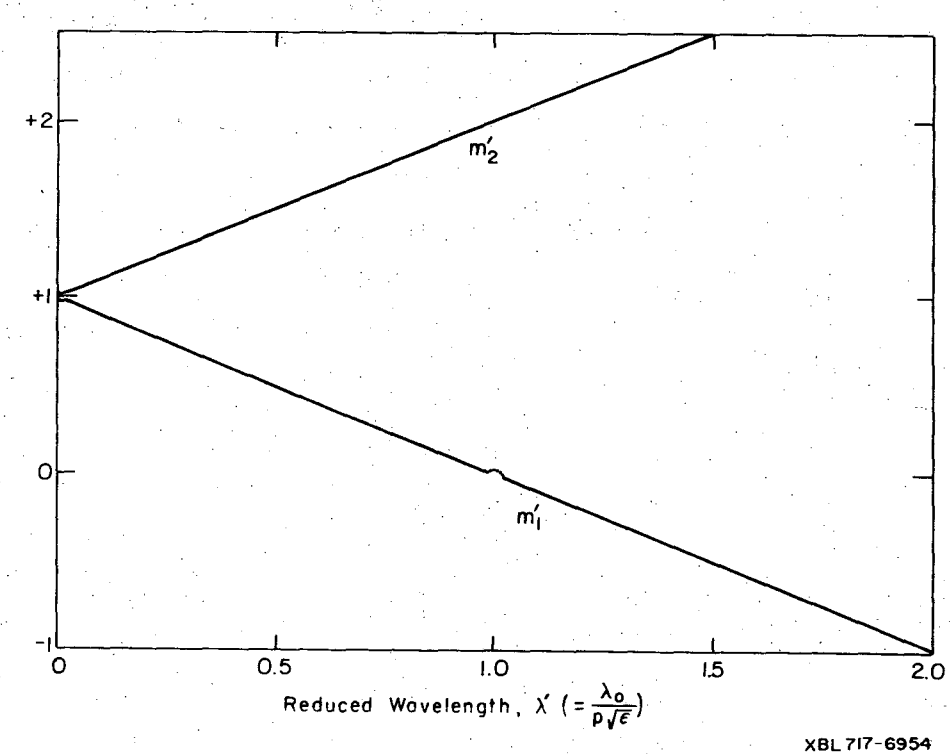

Fig. 3-1a

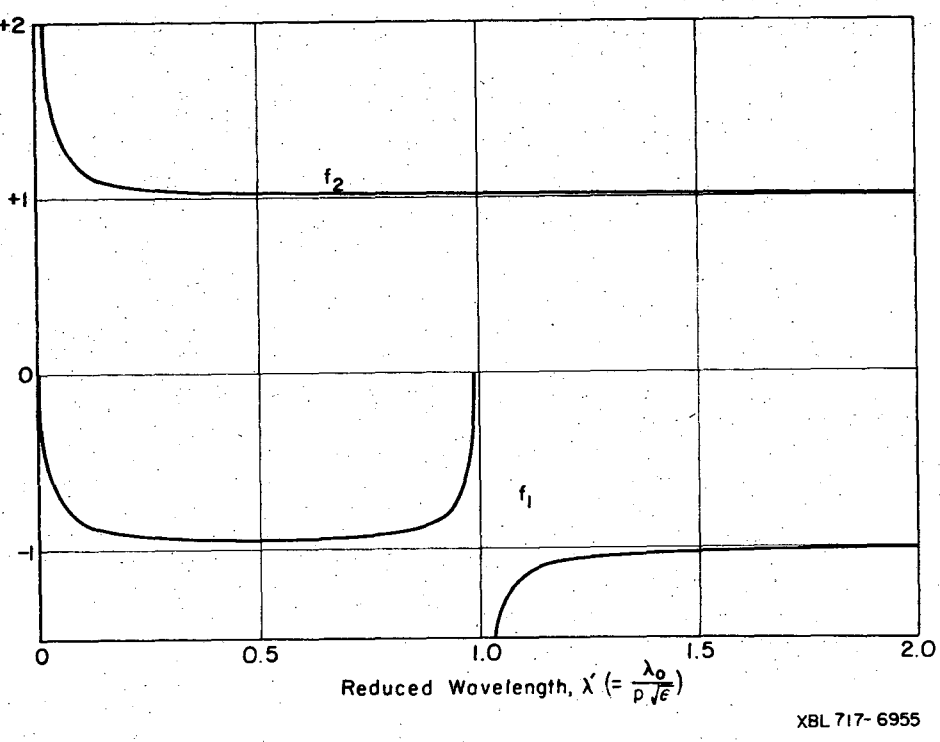

Fig. 3-1b

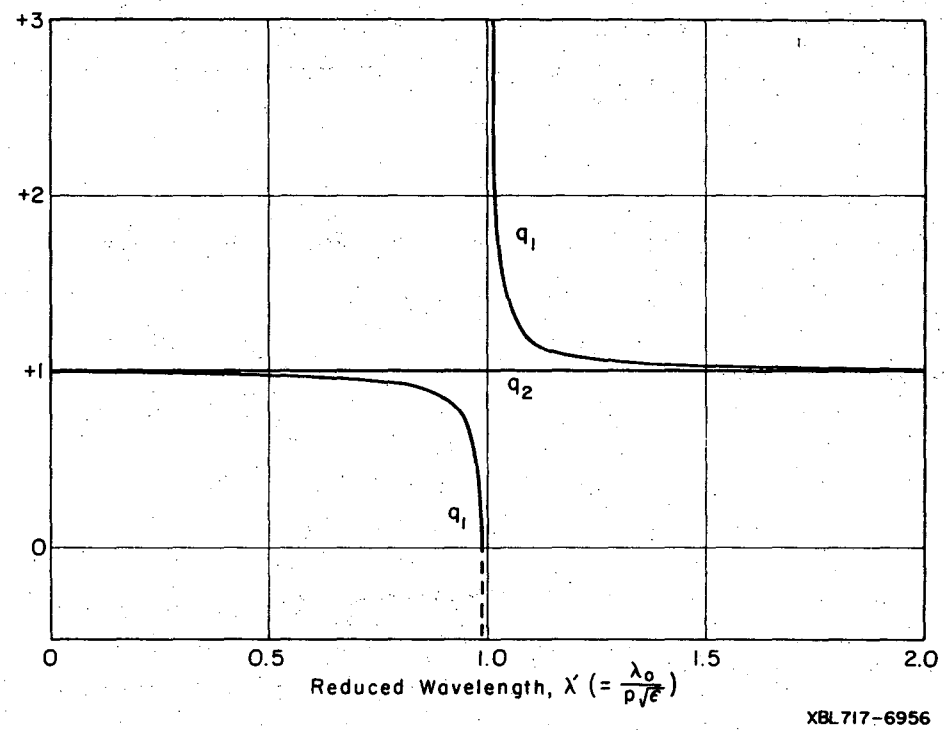

Fig. 3-1c

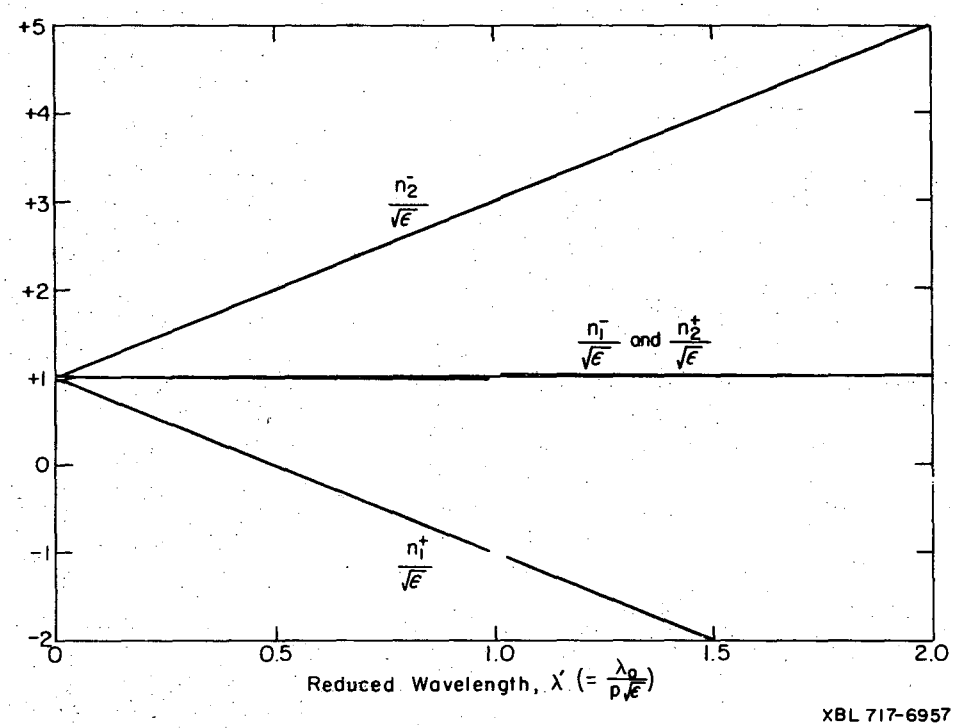

Fig. 3-2

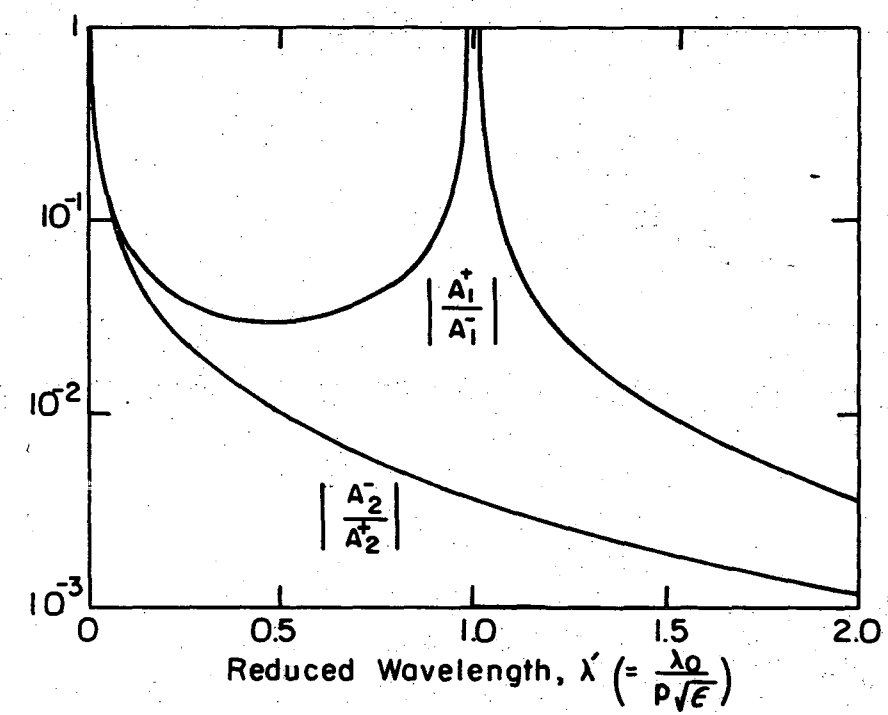

XBL 717-6958

Fig. 3-3

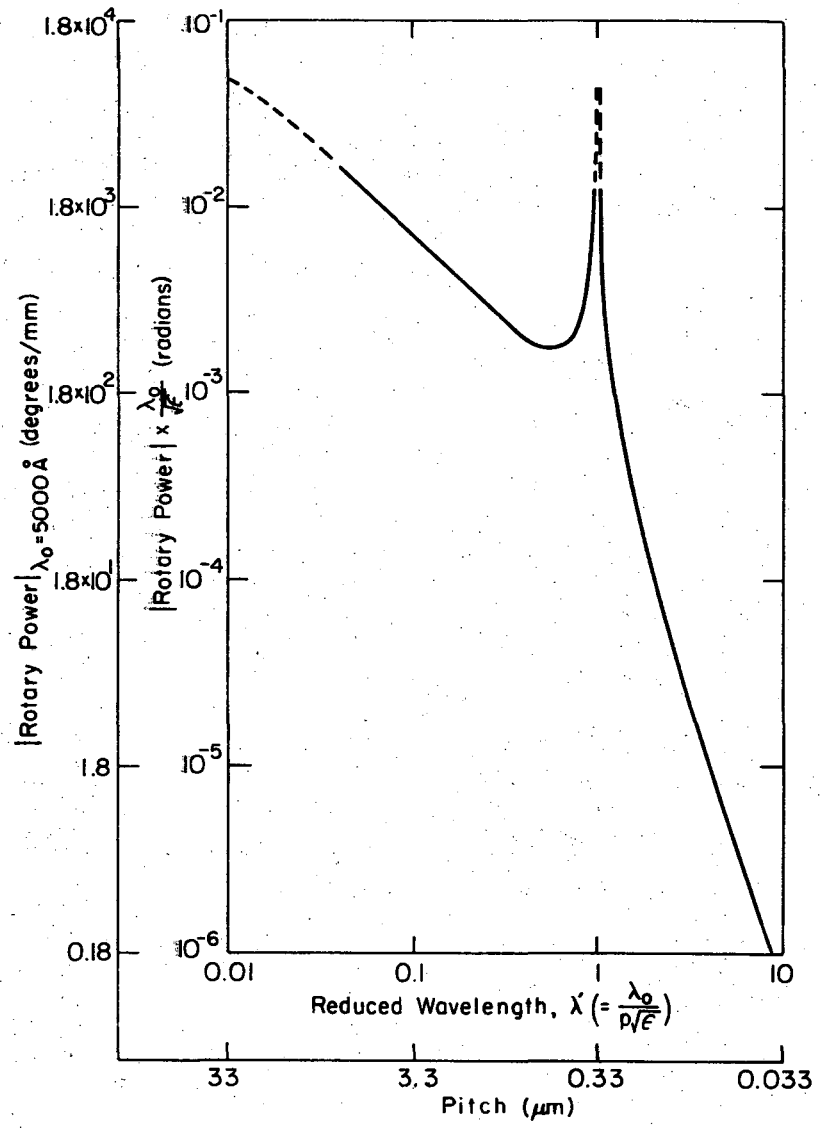

XBL 717-6959

Fig. 3-4

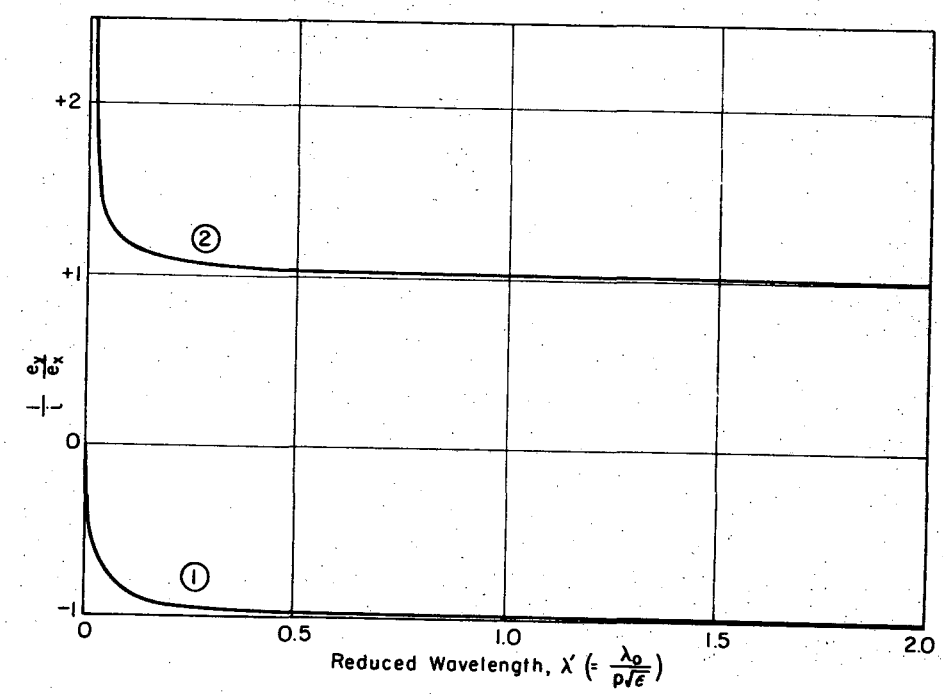

XBL 717-6960

Fig. 3-5

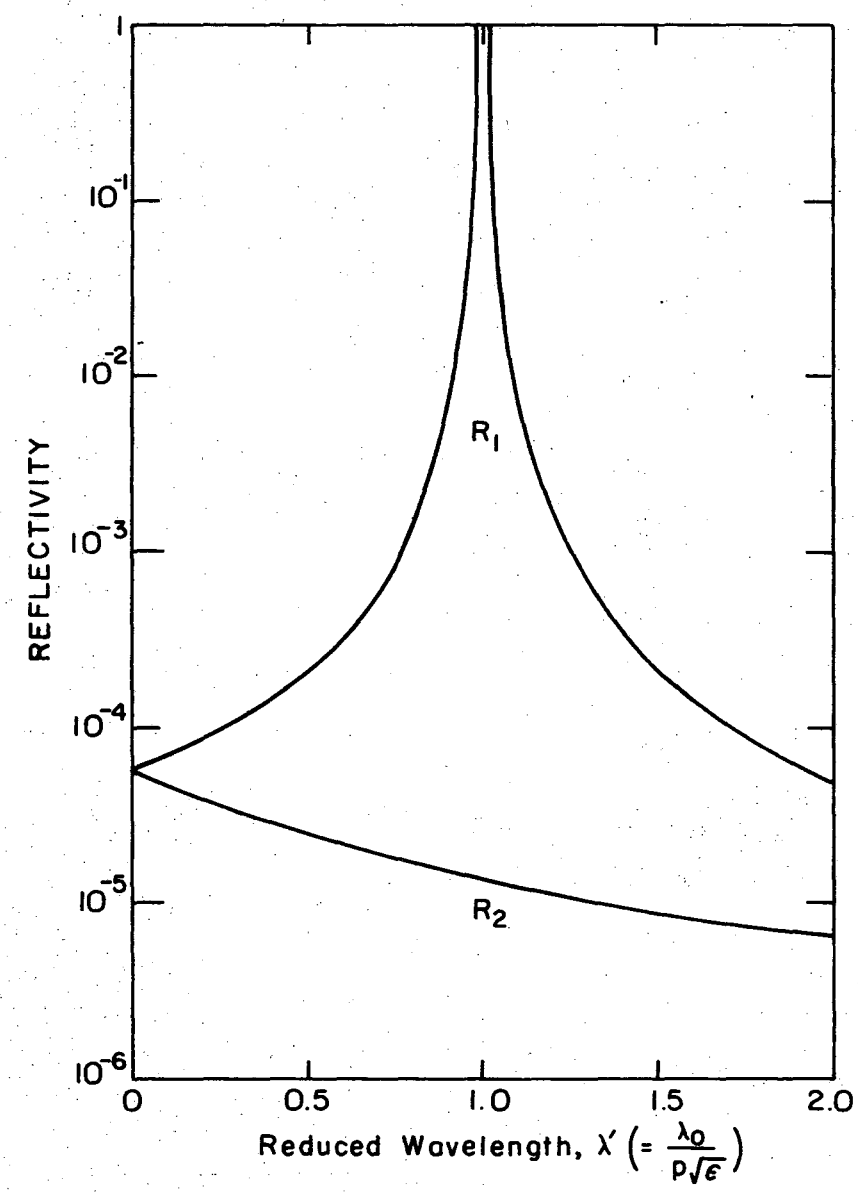

XBL717-6961

Fig. 3-6

IV. NON-LINEAR THEORY

For propagation of infinite plane waves along the helical axis (taken as the z axis) of a cholesteric medium, the wave equation in the laboratory frame, including non-linear sources, has the form

$$\left(\frac{\partial^2}{\partial z^2} + \left(\frac{3\omega}{c}\right)^2 \underset{\approx}{\varepsilon}(z,3\omega)\right) \underset{\sim}{E}(z,3\omega) = -4\pi\left(\frac{3\omega}{c}\right)^2 \underset{\sim}{P}^{NL}(z,3\omega), \qquad (4\text{-}1)$$

where $\underset{\sim}{E}(z,3\omega)$ is the electric field at frequency 3ω, $\underset{\approx}{\varepsilon}(z,3\omega)$ is the corresponding (linear) dielectric constant and $\underset{\sim}{P}^{NL}(z,3\omega)$ is the non-linear polarization at frequency 3ω. With the electric dipole approximation, the non-linear polarization for third-harmonic generation has the form

$$\underset{\sim}{P}^{NL}(z,3\omega) = \underset{\approx}{\chi}^{NL}\, \underset{\sim}{E}(z,\omega)\, \underset{\sim}{E}(z,\omega)\, \underset{\sim}{E}(z,\omega) \qquad (4\text{-}2)$$

where $\underset{\approx}{\chi}^{NL}$ is the corresponding non-linear susceptibility. In the laboratory, both $\underset{\approx}{\varepsilon}$ and $\underset{\approx}{\chi}^{NL}$ vary with z because of the changing direction of molecular alignment as a function of z. However in the twisted coordinate system ((ξ, η, z) - Eqs. (3-1) and (3-2)), the alignment direction does not change, and hence $\underset{\approx}{\varepsilon}$ and $\underset{\approx}{\chi}^{NL}$ are both constant. Application of the twist transformation, Eq. (3-2), to Eq. (4-1) yields the corresponding wave equation in the twisted coordinate system:

$$\left(\frac{\partial^2}{\partial z^2} + \frac{4\pi}{p}\,\underset{\approx}{\sigma}\,\frac{\partial}{\partial z} - \left(\frac{2\pi}{p}\right)^2 + \left(\frac{3\omega}{c}\right)^2 \underset{\approx}{\varepsilon}_T\right) \underset{\sim}{E}_T(z,3\omega) =$$

$$- 4\pi \left(\frac{3\omega}{c}\right)^2 \underset{\approx}{\chi}_T^{NL}\, \underset{\sim}{E}_T(z,\omega)\, \underset{\sim}{E}_T(z,\omega)\, \underset{\sim}{E}_T(z,\omega) \quad . \tag{4-3}$$

The forward propagating field at frequency 3ω is generally a linear combination of the two forward propagating modes,

$$\begin{aligned} \underset{\sim}{E}(z,3\omega) = {} & \mathcal{E}_1^{(3\omega)}(z)\, \hat{e}_1(3\omega)\, e^{ik_1^{(3\omega)}z} \\ & + \mathcal{E}_2^{(3\omega)}(z)\, \hat{e}_2(3\omega)\, e^{ik_2^{(3\omega)}z} \end{aligned} \tag{4-4}$$

where $\mathcal{E}_1(z)$ and $\mathcal{E}_2(z)$ are assumed to be slowly varying functions of z. (Solutions for the backward propagating third-harmonic waves may be obtained by inverting all propagation directions in the final solution, Eq. (4-12).) Substitution into Eq. (4-3) and using Eq. (3-9) yields

$$\begin{aligned} & \left(2ik_1 + \frac{4\pi}{p}\,\underset{\approx}{\sigma}\right) \hat{e}_1 e^{ik_1 z}\, \frac{\partial}{\partial z}\, \mathcal{E}_1(z) + \\ & \left(2ik_2 + \frac{4\pi}{p}\,\underset{\approx}{\sigma}\right) \hat{e}_2 e^{ik_2 z}\, \frac{\partial}{\partial z}\, \mathcal{E}_2(z) = \\ & \qquad - 4\pi \left(\frac{3\omega}{c}\right)^2 \underset{\sim}{P}_T^{NL}(z,3\omega) \ , \end{aligned} \tag{4-5}$$

where we have neglected the second derivatives of $\mathcal{E}_1(z)$ and $\mathcal{E}_2(z)$.

The scalar products of $\hat{e}_1^{\dagger}(3\omega)$ and $\hat{e}_2^{\dagger}(3\omega)$ (the conjugate transposes of $\hat{e}_1$ and $\hat{e}_2$) with Eq. (4-5) yield

$$\begin{aligned} & Ae^{ik_1 z}\, \frac{\partial}{\partial z}\, \mathcal{E}_1(z) + Be^{ik_2 z}\, \frac{\partial}{\partial z}\, \mathcal{E}_2(z) = \\ & \qquad \frac{2i\pi(3\omega)}{c\sqrt{\varepsilon(3\omega)}}\, \hat{e}_1^{\dagger}(3\omega) \cdot \underset{\sim}{P}_T^{NL}(z,3\omega) \end{aligned} \tag{4-6a}$$

$$\begin{aligned} & Ce^{ik_2 z}\, \frac{\partial}{\partial z}\, \mathcal{E}_2(z) + De^{ik_2 z}\, \frac{\partial}{\partial z}\, \mathcal{E}_2(z) = \\ & \qquad \frac{2i\pi(3\omega)}{c\sqrt{\varepsilon(3\omega)}}\, \hat{e}_2^{\dagger}(3\omega) \cdot \underset{\sim}{P}_T^{NL}(z,3\omega) \ , \end{aligned} \tag{4-6b}$$

where

$$A = m_1' - 2\lambda' \frac{\mathrm{Re}(f_1)}{1+|f_1|^2} \tag{4-7a}$$

$$B = [m_2'(1 + f_1^* f_2) - \lambda'(f_1^* + f_2)] / \sqrt{(1+|f_1|^2)(1+f_2^2)} \tag{4-7b}$$

$$C = [m_1'(1 + f_1 f_2) - \lambda'(f_1 + f_2)] / \sqrt{(1+|f_1|^2)(1+f_2^2)} \tag{4-7c}$$

$$D = m_2' - 2\lambda' \frac{f_2}{1+f_2^2} \ , \tag{4-7d}$$

and where the parameters m' and f are to be evaluated at frequency 3ω.

Hence

$$\frac{\partial}{\partial z}\,\mathcal{E}_1(z) = \frac{2i\pi(3\omega)}{c\sqrt{\varepsilon}}\left(\frac{D\hat{e}_1^{\dagger} - B\hat{e}_2^{\dagger}}{AD - BC}\right)\cdot \underset{\sim}{p}^{NL}(z,3\omega)\, e^{-ik_1 z} \qquad (4\text{-}8a)$$

$$\frac{\partial}{\partial z}\,\mathcal{E}_2(z) = \frac{2i\pi(3\omega)}{c\sqrt{\varepsilon}}\left(\frac{A\hat{e}_2^{\dagger} - C\hat{e}_1^{\dagger}}{AD - BC}\right)\cdot \underset{\sim}{p}^{NL}(z,3\omega)\, e^{-ik_2 z} \qquad (4\text{-}8b)$$

The fact that the components of $\underset{\sim}{p}^{NL}$ in the directions of <u>both</u> normal-mode polarizations radiate into <u>each</u> normal mode is a consequence of the lack of orthogonality between the modes (Eq. (3-37)).

Assuming that the driving field at frequency ω is not depleted, $\underset{\sim}{E}_T(z,\omega)$ in Eq. (4-3) can be expressed as a superposition of the four normal modes at frequency ω (two propagating forward and two backward).

$$\mathcal{E}_1^{(\omega)}(z,\omega) = \sum_{\ell} \mathcal{E}_{\ell}^{(\omega)}\, \hat{e}_{\ell}(\omega)\, e^{ik_{\ell}^{(\omega)} z} \qquad (4\text{-}9)$$

Integration of Eq. (4-8) then yields

$$\mathcal{E}_1^{(3\omega)}(z) = \frac{2i\pi(3\omega)}{c\sqrt{\varepsilon}}\left(\frac{D\hat{e}_1^{\dagger}(3\omega) - B\hat{e}_2^{\dagger}(3\omega)}{AD - BC}\right)\cdot \underset{\approx}{\chi}^{NL} :$$

$$\sum_{\ell,m,n} \hat{e}_{\ell}(\omega)\, \hat{e}_m(\omega)\, \hat{e}_n(\omega)\, \mathcal{E}_{\ell}^{(\omega)}\, \mathcal{E}_m^{(\omega)}\, \mathcal{E}_n^{(\omega)} \times$$

$$\frac{\sin\left(\frac{1}{2}(\Delta k)_{1\ell mn} z\right)}{\frac{1}{2}(\Delta k)_{1\ell mn}}\; e^{-i\frac{1}{2}(\Delta k)_{1\ell mn} z} \qquad (4\text{-}10a)$$

$$\mathcal{E}_2^{(3\omega)}(z) = \frac{2\pi i(3\omega)}{c\sqrt{\varepsilon}}\left(\frac{A\hat{e}_2^{\dagger}(3\omega) - C\hat{e}_1^{\dagger}(3\omega)}{AD - BC}\right)\cdot \underset{\approx}{\chi}^{NL} :$$

$$\sum_{\ell,m,n} \hat{e}_{\ell}(\omega)\, \hat{e}_m(\omega)\, \hat{e}_n(\omega)\, \mathcal{E}_{\ell}^{(\omega)}\, \mathcal{E}_m^{(\omega)}\, \mathcal{E}_n^{(\omega)} \times$$

$$\frac{\sin\left(\frac{1}{2}(\Delta k)_{2\ell mn} z\right)}{\frac{1}{2}(\Delta k)_{2\ell mn}}\; e^{-i\frac{1}{2}(\Delta k)_{2\ell mn} z} \qquad (4\text{-}10b)$$

with

$$(\Delta k)_{j\ell mn} = k_j^{(3\omega)} - k_{\ell}^{(\omega)} - k_m^{(\omega)} - k_n^{(\omega)} \qquad (4\text{-}11)$$

If one particular combination (ℓ, m, n) of fundamental-frequency modes is dominant, for instance due to experimentally chosen incident polarizations and/or due to phase matching ($\Delta k = 0$, see below) we can neglect all other terms in the sum. Then, using the expression for the time averaged Poynting's vector derived in the previous section, Eq. (3-19), we obtain for the third-harmonic intensity in either of two forward modes at the end of a sample of thickness z (neglecting boundary reflections)

$$I_1^{(3\omega)}(z) = \frac{\pi\,(3\omega)^2}{2c\,\sqrt{\varepsilon(3\omega)}} \cdot \frac{\mathrm{Re}\left(q_1(3\omega) + \dfrac{|f_1(3\omega)|^2}{q_1(3\omega)}\right)}{1 + |f_1(3\omega)|^2} \times$$

$$\left|\left(\frac{D\hat{e}_1^{\dagger}(3\omega) - B\hat{e}_2^{\dagger}(3\omega)}{AD - BC}\right) \cdot \underset{\approx}{\chi}^{NL} : \hat{e}_\ell(\omega)\,\hat{e}_m(\omega)\,\hat{e}_n(\omega)\right|^2 \times$$

$$\left|\mathcal{E}_\ell^{(\omega)}\,\mathcal{E}_m^{(\omega)}\,\mathcal{E}_n^{(\omega)}\right|^2 \frac{\mathrm{Sin}^2\left(\frac{1}{2}(\Delta k)_{1\ell mn} z\right)}{\left(\frac{1}{2}(\Delta k)_{1\ell mn}\right)^2} \qquad (4\text{-}12a)$$

$$I_2^{(3\omega)}(z) = \frac{\pi\,(3\omega)^2}{2c\,\sqrt{\varepsilon(3\omega)}} \left(\frac{q_2(3\omega) + \dfrac{f_2^{\,2}(3\omega)}{q_2(3\omega)}}{1 + f_2^{\,2}(3\omega)}\right) \times$$

$$\left|\left(\frac{A\hat{e}_2^{\dagger}(3\omega) - C\hat{e}_1^{\dagger}(3\omega)}{AD - BC}\right) \cdot \underset{\approx}{\chi}^{NL} : \hat{e}_\ell(\omega)\,\hat{e}_m(\omega)\,\hat{e}_n(\omega)\right|^2 \times$$

$$\left|\mathcal{E}_\ell^{(\omega)}\,\mathcal{E}_m^{(\omega)}\,\mathcal{E}_n^{(\omega)}\right|^2 \frac{\mathrm{Sin}^2\left(\frac{1}{2}(\Delta k)_{2\ell mn} z\right)}{\left(\frac{1}{2}(\Delta k)_{2\ell mn}\right)^2} \qquad (4\text{-}12b)$$

Third-harmonic generation is most efficient when the phase-matching condition $(\Delta k)_{j\ell mn} = 0$ is satisfied. Given ω, ε and α, one can compute from Eqs. (3-10) - (3-11) and (4-11) the phase mismatch (Δk) for all mode combinations at all pitches. Because of the strong dependence of k on pitch (Fig. 3-1a) and the fact that the pitch of cholesteric materials is a continuously variable parameter over a large region (2200 Å $< |p| < \infty$), phase-matched third-harmonic

generation can in fact be achieved in principle for at least fourteen different mode combinations. Table 4-1 lists all these possible phase-matching conditions for third-harmonic generation from 1.06 μm waves propagating along the helical axis of a twisted birefringent medium with ordinary dispersion.

The phase-matched mode combinations involving waves propagating both forwards and backwards have no analogues in homogeneous media. There is an apparent lack of conservation of linear momentum among the interacting waves. Phase matching in these cases can be understood in terms of the periodicity of the medium. Since the periodicity of the linear and third-order optical properties is p/2 the unit lattice momentum is $(4\pi/p)\,\hbar$. Hence we can expect momentum in multiples of this unit to be echanged with the medium.[17,18] In the limit that the birefringence α is negligible in the expressions for k, we have from Eqs. (3-10) and (3-12)

$$k_1 \cong k_o - \frac{2\pi}{p} \qquad (4\text{-}13a)$$

$$k_2 \cong k_o + \frac{2\pi}{p} \qquad (4\text{-}13b)$$

where $k_o = \frac{\omega}{c}\sqrt{\varepsilon}$ and $\varepsilon = (\varepsilon_\xi + \varepsilon_\eta)/2$.

Using this approximation the phase-matching condition for the fifth mode combination, for example, in Table 4-1,

$$k_2^{(\omega)} + k_2^{(\omega)} + k_{\bar{1}}^{(\omega)} = k_1^{(3\omega)} \qquad (4\text{-}14)$$

reduces to

$$k_o^{(\omega)} + k_o^{(\omega)} + (-k_o^{(\omega)}) \cong k_o^{3\omega} - 2\frac{4\pi}{p} \qquad (4\text{-}15)$$

Hence the apparent laboratory-frame momentum mismatch among the optical fields is accounted for by two units of the lattice momentum. Analagous results can be obtained for all the mixed-direction mode combinations. One can compute from Eq. (4-15) the approximate pitch for phase-matching of the corresponding mode combination: $k_o^{(\omega)} \simeq 9\ \mu m^{-1}$ and $k_o^{(3\omega)} \simeq 27\ \mu m^{-1}$ giving $p \simeq 1.4\ \mu m$, in agreement with the value in Table 4-1.

Similar considerations are applicable for angular momentum. For small α the two normal modes are approximately circularly polarized in opposite senses in the laboratory frame (except for $\lambda' \lesssim \alpha$). Thus photons in the two forward modes carry equal and opposite units of angular momentum ($\pm\hbar$), with the signs reversed for the backward propagating modes. For the tenth mode combination, for example, in Table 4-1, the consequent angular-momentum mismatch among the fields is $4\hbar$. But since the medium has two-fold rotational symmetry about the z-axis (see below), the fields can exchange angular momentum with the medium in units of $2\hbar$. Examination of all the mode combinations in Table 4, assuming the modes are circularly polarized, shows that the angular momentum mismatch among the optical fields is always an interger multiple of $2\hbar$ and hence can be accounted for by exchange with the medium.

All of the phase-matched mode combinations can also be understood in analogy with electrons propagating in a one-dimensional periodic lattice. We can express the normal modes in Bloch-function

form (Eq. (3-39))

$$\underset{\sim}{E}(z) = e^{i\kappa z}\, u_\kappa(z). \qquad (4\text{-}16)$$

κ is given modulo $\frac{4\pi}{p}$ in Eq. (3-48). It is customary to make κ unique by requiring that it lie in the first Brillouin zone, $-2\pi/p < \kappa < 2\pi/p$.[17,18] Consequently, for example for the tenth mode combination, which is phase matched for $p \simeq 0.47\ \mu$, we have $\kappa_1 = k_1 + \frac{2\pi}{p}$. Then the corresponding phase-matching condition,

$$k_1^{(\omega)} + k_1^{(\omega)} + k_1^{(\omega)} = (-k_1^{(3\omega)}) \qquad (4\text{-}17)$$

can be written equivalently as

$$\kappa_1^{(\omega)} + \kappa_1^{(\omega)} + \kappa_1^{(\omega)} = (-\kappa_1^{(3\omega)}) + \frac{4\pi}{p} \qquad (4\text{-}18)$$

The occurrence of a reciprocal lattice vector (integer multiple of $4\pi/p$) is the definition of an umklapp process.[31] Thus this mode combination, as well as #6 and #14, generate third harmonic fields via a coherent optical umklapp process. For all the other mode combinations no reciprocal lattice vector appears in the expressions analagous to Eq. (4-18) and hence their harmonic generation would be called "ordinary" processes.[31]

One final interpretation of the phase matching conditions may be useful. As indicated in Eqs. (3-23) - (3-25), <u>each</u> normal mode made be written (exactly) in the laboratory frame as a linear superposition of left-and right circularly polarized waves each with

its own amplitude $A_{1,2}^{+,-}$ (Fig. 3-3) and effective refractive index $n_{1,2}^{+,-}$ (Fig. 3-2). Since the normal modes themselves are nearly circularly polarized for most values of λ', the amplitude of one of the circularly-polarized components of each mode is much larger than the other. But the weak amplitude components play critical roles in achieving phase matching. If the four non-zero elements of $\underset{\approx}{\chi}^{NL}$ (Eqs. (4-26) and (4-27)) are equal (see Section VI), the non-linear tensor has the same form as for third-harmonic generation in isotropic media and it is independent of z in the laboratory frame. Hence linear and angular momentum are conserved among the electromagnetic waves inside the medium, without exchange with the lattice. Then if one treats each circularly-polarized component of each normal mode as independent and searches for all possible phase-matching conditions for third-harmonic generation, consistent with angular momentum conservation, one obtains a list corresponding exactly to that in Table 4-1. For instance for mode combination #4 in Table 4-1,

$$\mathcal{E}_2(3\omega) \propto \mathcal{E}_2(\omega)\ \mathcal{E}_2(\omega)\ \mathcal{E}_2(\omega) \tag{4-19a}$$

$$3m_2(3\omega) = m_2(\omega) + m_2(\omega) + m_2(\omega)\ , \tag{4-19b}$$

we obtain

$$A_2^{\pm}(3\omega) \propto A_2^{\pm}(\omega)A_2^{\pm}(\omega)\ A_2^{\mp}(\omega) \tag{4-20a}$$

$$3n_2^{\pm}(3\omega) = n_2^{\pm}(\omega) + n_2^{\pm}(\omega) + n_2^{\mp}(\omega). \tag{4-20b}$$

Since $n_2^{\pm}(\omega) = m_2(\omega) \mp \dfrac{\lambda^{(\omega)}}{p}$, the two phase-matching conditions (Eqs. 4-19b and 4-20b) are exactly equivalent. In addition to yielding the phase-matching conditions exactly, this picture provides an easy way to estimate the relative intensities of the third-harmonic signal generated with the various mode combinations, simply by computing the relative amplitudes $A_{1,2}^{+,-}$ of the relevant circularly polarized components of the modes. Phase-matched mode combinations involving very weak circularly-polarized components of some of the modes (necessary to conserve angular momentum) will be relatively inefficient in converting the laser light to its third harmonic. Such estimates of course will be accurate only to the extent that the non-zero elements of $\underset{\approx}{\chi}^{NL}$ in fact are equal. Our experiments indicate that to a first rough approximation this is indeed the case for our liquid-crystal samples.

Some of these phase-matchable mode combinations have correspondences in untwisted media. The second combination in Table 4-1 is

$$\mathcal{E}_1^{(3\omega)} \propto \mathcal{E}_1^{(\omega)}\ \mathcal{E}_2^{(\omega)}\ \mathcal{E}_2^{(\omega)} \tag{4-21a}$$

$$k_1^{(3\omega)} = k_1^{(\omega)} + k_2^{(\omega)} + k_2^{(\omega)} \tag{4-21b}$$

In the limit $p \to \infty$ where $\hat{e}_1 = \hat{\xi} = \hat{x}$ and $\hat{e}_2 = \hat{\eta} = \hat{y}$, Eq. (4-21) become

$$\mathcal{E}_x^{(3\omega)} \propto \mathcal{E}_x^{(\omega)}\ \mathcal{E}_y^{(\omega)}\ \mathcal{E}_y^{(\omega)} \tag{4-22a}$$

$$n_x(3\omega) - n_x(\omega) = \frac{2}{3}\,(n_y(\omega) - n_x(\omega)). \tag{4-22b}$$

The phase-matching condition has been rearranged to illustrate the compensation of the color dispersion by linear birefringence. This is the most common laboratory technique for achieving phase-matching.

In the regions of pitch where the normal modes at both ω and 3ω are approximately circularly polarized we have $\hat{e}_1 \simeq \frac{1}{\sqrt{2}}(\hat{x} - i\hat{y}) \equiv \hat{-}$ and $\hat{e}_2 \simeq \frac{1}{\sqrt{2}}(\hat{x} + i\hat{y}) \equiv \hat{+}$ (for $p > 0$). Then the third mode combination in Table 4-1,

$$\mathcal{E}_1^{(3\omega)} \propto \mathcal{E}_1^{(\omega)} \; \mathcal{E}_1^{(\omega)} \; \mathcal{E}_2^{(\omega)} \tag{4-23a}$$

$$k_1^{(3\omega)} = k_1^{(\omega)} + k_1^{(\omega)} + k_2^{(\omega)} \tag{4-23b}$$

can be described approximately by

$$\mathcal{E}_-^{(3\omega)} \propto \mathcal{E}_-^{(\omega)} \; \mathcal{E}_-^{(\omega)} \; \mathcal{E}_+^{(\omega)} \tag{4-24a}$$

$$m_-^{(3\omega)} - m_-^{(\omega)} \simeq \frac{1}{3}\left(m_+^{(\omega)} - m_-^{(\omega)}\right) \tag{4-24b}$$

Physically, the color dispersion is compensated by its circular birefringence or rotary power in the twisted coordinate system. This phase-matching technique,[6] applied to difference-frequency generation, has observed in optically active materials.[7]

We were unable to observe third-harmonic generation phase matched by circular-birefringent compensation in cholesteric liquid crystals despite their extraordinarily high optical rotary power (or circular birefringence).[8,9,32] Mode combination #3 (discussed above) was not phase-matchable in our cholesteric materials because

the values of the parameters ε and α did not satisfy the inequality in Table 4-1. But even if the inequality were satisfied, the resulting phase matching could not be properly attributed to circular-birefringent compensation unless phase-matching occurred at a pitch such that the normal modes at both ω and 3ω were nearly circularly polarized, so that the medium could indeed be characterized by circular birefringence. If the inequality is satisfied as an equality, the phase-matching pitch is ∞, and the normal modes are linearly polarized. For $\alpha \approx 0.03$ (typical for our materials), the color dispersion ($\varepsilon(1.06\ \mu m) - \varepsilon(0.35\ \mu m)$) would have to be ~ 0.001, one tenth of the actual value in our materials, in order to achieve phase-matched third-harmonic generation via circular-birefringent compensation.

In the twisted-frame coordinates $(\hat{\xi}, \hat{\eta})$ the only relevant elements of $\underset{\approx}{\chi}^{NL}$ are

$$\begin{matrix} \chi_{\xi\xi\xi\xi} & \chi_{\xi\xi\xi\eta} & \chi_{\xi\xi\eta\eta} & \chi_{\xi\eta\eta\eta} \\ \chi_{\eta\xi\xi\xi} & \chi_{\eta\eta\xi\xi} & \chi_{\eta\eta\eta\xi} & \chi_{\eta\eta\eta\eta} \end{matrix} \tag{4-25}$$

(Elements differing by permutations of the last three indices are equal; this degeneracy has not been included in this list.) The medium is homogeneous, with all molecules aligned parallel or anti-parallel to each other. The molecules themselves lack inversion symmetry, so that if they were all aligned pointing the same direction it would be possible to generate second harmonic. The lack of observed second-harmonic generation in cholesteric media[11-13,33] implies that the medium has a high degree of inversion symmetry and hence

that the molecules may be alignen with equal "up" and "down" orientations. This would imply the medium has reflection symmetries across both the ξ and η axes and hence only four elements of $\underset{\approx}{\chi}^{NL}$ in Eq. (4-25) are non-vanishing. They are

$$
\begin{aligned}
C_{11} &\equiv \chi_{\xi\,\xi\,\xi\,\xi} \\
C_{12} &\equiv 3\chi_{\xi\,\xi\,\eta\,\eta} \\
C_{21} &\equiv 3\chi_{\eta\,\eta\,\xi\,\xi} \\
C_{22} &\equiv \chi_{\eta\,\eta\,\eta\,\eta}
\end{aligned}
\qquad (4\text{-}26)
$$

The non-linear polarization along $\hat{\xi}$ and $\hat{\eta}$ in the twisted frame are therefore given by

$$P_{\xi}^{NL}(3\omega) = C_{11} E_{\xi}^{(\omega)} E_{\xi}^{(\omega)} E_{\xi}^{(\omega)} + C_{12} E_{\xi}^{(\omega)} E_{\eta}^{(\omega)} E_{\eta}^{(\omega)} \qquad (4\text{-}27a)$$

$$P_{\eta}^{NL}(3\omega) = C_{21} E_{\eta}^{(\omega)} E_{\xi}^{(\omega)} E_{\xi}^{(\omega)} + C_{22} E_{\eta}^{(\omega)} E_{\eta}^{(\omega)} E_{\eta}^{(\omega)} \qquad (4\text{-}27b)$$

Experimentally we measure the components of $\underset{\approx}{\chi}^{NL}$ in Eq. (4-12). These components can be expressed in terms of C_{11}, C_{12}, C_{21} and C_{22} using the relation (obtained from Eqs. (3-8) and (3-11)

$$\hat{e}_{\ell}(\omega) = \frac{1}{\sqrt{1 + |f_{\ell}(\omega)|^2}} \left(\hat{\xi} + i f_{\ell}\, \hat{\eta}\right) . \qquad (4\text{-}28)$$

The results are given in Table 4-2.

It is clear that since C_{11}, C_{12}, C_{21} and C_{22} are all non-vanishing, phase-matched third-harmonic generation should exist for all the mode combinations in Table 4-1. In principle the relative values of C_{11}, C_{12}, C_{21} and C_{22} can be determined by measuring the relative third harmonic intensity generated via four (or more) different mode combinations. In our experiments we used different mixtures of cholesteric materials and/or different temperatures to observe most of the different mode combinations, and hence the non-linear susceptibility may be different for these combinations. However the temperature effect should be very small over our ~ 30°C range and experimentally we find our data is consistent with $\underset{\approx}{\chi}^{NL}$ being nearly the same for all our different mixtures. This is reasonable in light of the large size of each type of molecule and the lack of any radically different structure or bonding in the various groups added to cholesterol to make the cholesteric liquid crystalline materials we used (see next section).

Table 4-1. All mode combinations which are phase-matchable for third-harmonic generation from 1.06 μm fundamental. The bars indicate backward modes (with Poynting vector in -z direction). The possiblity of phase-matching for the first three mode combinations is very sensitive to the medium parameters ε and α. All the other mode combinations are phase-matchable at some (not the same) pitch for any medium parameters in the range investigated, namely $0<\alpha<0.5$, $0<\varepsilon(3\omega) - \varepsilon(\omega) < 0.2$ and $1 < \frac{1}{2}(\varepsilon(3\omega) + \varepsilon(\omega)) < 4$. The particular pitches for phase matching given in the table are for $\alpha = 0.03$, $\varepsilon(\omega) = 2.18$ and $\varepsilon(3\omega) = 2.30$, which are typical for our experimental materials. The possibility of anomolous dispersion between ω and 3ω has not been included in this table.

Table 4-1

Mode Combination (ω → 3ω)	Condition For Existence of Phase Matching	Approximate Pitch For Phase Matching (μm)
1. 222 → 1	$(\varepsilon(3\omega)/\varepsilon(\omega) - 1) \gtrsim \alpha$	
2. 122 → 1	$(\varepsilon(3\omega)/\varepsilon(\omega) - 1) \gtrsim \frac{2}{3}\alpha$	
3. 112 → 1	$(\varepsilon(3\omega)/\varepsilon(\omega) - 1) \lesssim \frac{1}{3}\alpha$	
4. 222 → 2		17
5. 22$\bar{1}$ → 1		1.4
6. 11$\bar{2}$ → $\bar{1}$		0.70
7. 22$\bar{2}$ → 1		0.69
8. 21$\bar{1}$ → 1		0.69
9. 22$\bar{1}$ → 2		0.69
10. 111 → $\bar{1}$		0.47
11. 11$\bar{1}$ → $\bar{1}$		0.35
12. 12$\bar{2}$ → $\bar{1}$		0.35
13. 11$\bar{2}$ → $\bar{2}$		0.35
14. 111 → $\bar{2}$		0.24

Table 4-2 The components of $\underset{\approx}{\chi}^{NL}$ which appear in Eq. (4-12) in terms of the non-zero elements of $\underset{\approx}{\chi}^{NL}$ in the twisted coordinates (Eq. (4-26)). Each expression in the first column is equal to the linear combination of c's indicated in the other four columns; e.g.,

$$\chi_{j\,111} \Big/ \left(N_j(3\omega)\, N_1^{\,3}(\omega)\right) = C_{11} - f_1^{\,2}(\omega)\, C_{12}$$

$$+ f_j(3\omega)\, f_1(\omega)\, C_{21} - f_j(3\omega)\, f_1^{\,3}(\omega)\, C_{22}$$

j designates any of the four third-harmonic modes. $\chi_{j\ell mn}$ is invariant under reversal of all propagation directions; e.g., $\chi_{\bar{1}\,111} = \chi_{1\,\bar{1}\bar{1}\bar{1}}$.

Table 4-2

	C_{11}	C_{12}	C_{21}	C_{22}
$\chi_{j\,111}/N_j(3\omega)\,N_1^{\,3}(\omega))$	1	$-f_1^{\,2}(\omega)$	$f_j(3\omega)\,f_1(\omega)$	$-f_j(3\omega)\,f_1^{\,3}(\omega)$
$\chi_{j\,112}/(N_j(3\omega)\,N_1^{\,2}(\omega)\,N_2(\omega))$	3	$-f_1(\omega)(f_1(\omega)+2f_2(\omega))$	$f_j(3\omega)(2f_1(\omega)+f_2(\omega))$	$-3f_j(3\omega)\,f_1^{\,2}(\omega)\,f_2(\omega)$
$\chi_{j\,122}/(N_j(3\omega)\,N_1(\omega)\,N_2^{\,2}(\omega)$	3	$-f_2(\omega)(2f_1(\omega)+f_2(\omega))$	$f_j(3\omega)(f_1(\omega)+2f_2(\omega))$	$-3f_j(3\omega)\,f_1(\omega)\,f_2^{\,2}(\omega)$
$\chi_{j\,222}/(N_j(3\omega)\,N_2^{\,3}(\omega))$	1	$-f_2^{\,2}(\omega)$	$f_j(3\omega)\,f_2(\omega)$	$-f_j(3\omega)\,f_2^{\,3}(\omega)$
$\chi_{j\,11\bar{1}}/(N_j(3\omega)\,N_1^{\,3}(\omega))$	3	$f_1^{\,2}(\omega)$	$f_j(3\omega)\,f_1(\omega)$	$3f_j(3\omega)\,f_1^{\,3}(\omega)$
$\chi_{j\,11\bar{2}}/(N_j(3\omega)\,N_1^{\,2}(\omega)\,N_2(\omega))$	3	$f_1(\omega)(2f_2(\omega)-f_1(\omega))$	$f_j(3\omega)(2f_1(\omega)-f_2(\omega))$	$3f_j(3\omega)\,f_1^{\,2}(\omega)\,f_2(\omega)$
$\chi_{j\,22\bar{1}}/N_j(3\omega)\,N_1(\omega)\,N_2^{\,2}(\omega))$	3	$f_2(\omega)(2f_1(\omega)-f_2(\omega))$	$f_j(3\omega)(2f_2(\omega)-f_1(\omega))$	$3f_j(3\omega)\,f_1(\omega)\,f_2^{\,2}(\omega)$
$\chi_{j\,22\bar{2}}/(N_j(3\omega)\,N_2^{\,3}(\omega))$	3	$f_2^{\,2}(\omega)$	$f_j(3\omega)\,f_2(\omega)$	$3f_j(3\omega)\,f_2^{\,3}(\omega)$
$\chi_{j\,1\bar{1}2}/(N_j(3\omega)\,N_1^{\,2}(\omega)\,N_2(\omega))$	6	$2f_1^{\,2}(\omega)$	$2f_j(3\omega)\,f_2(\omega)$	$6f_j(3\omega)\,f_1^{\,2}(\omega)\,f_2(\omega)$
$\chi_{j\,2\bar{2}1}/(N_j(3\omega)\,N_1(\omega)\,N_2^{\,2}(\omega))$	6	$2f_2^{\,2}(\omega)$	$2f_j(3\omega)\,f_1(\omega)$	$6f_j(3\omega)\,f_1(\omega)\,f_2^{\,2}(\omega)$

$$\chi_{j\ell mn} \equiv \hat{e}_j^{\,+}(3\omega)\cdot \underset{\approx}{\chi}^{NL} : \hat{e}_\ell(\omega)\,\hat{e}_m(\omega)\,\hat{e}_n(\omega) \qquad N_\ell(\omega') = \frac{1}{\sqrt{1+|f_\ell(\omega')|^2}}$$

V. EXPERIMENTS

In our experiments we have used a number of different cholesteric liquid-crystalline materials in order to observe the various predicted peaks in third-harmonic generation. Our observations of the mode combination 2,2, 2 → 2 (#4 in Table 4-1) were done using a mixture of 1.75: 1.00 by weight of cholesteryl chloride and cholesteryl myristate.[34] This mixture has the advantage of having a pitch which is variable from -1.7 μm to ± ∞ to + 2 μm by varying the temperature from 20 to 68°C. (A negative pitch denotes a left-handed twisted structure.) In particular, the samples could be tuned to both -17.3 and + 17.5 μm, the phase-matching pitches for mode combination #4 in Table 4-1 allowing verification of the predicted polarization reversals when the helicty of the structure changes.

All the other phase-matching peaks we observed required cholesteric structures with pitches < 1.5 μm. We used mixtures of cholesteryl oleyl carbonate, cholesteryl nonanoate (also called cholesteryl pelargonate) and cholesteryl chloride.[34] The particular mixtures were chosen for the accessibility of the desired pitch at a convenient temperature and for the convenience of a weak temperature depence of pitch, in order to decrease the criticality of temperature control. The ratio of cholesteryl oleyl carbonate to cholesteryl nonanoate (by weight) is unity in all our mixtures and the ratio of cholesteryl chloride to the sum of these two components varies. Fig. 5-1 shows how the pitch changes as a function of the concentration of cholesteryl chloride. The temperature variation of the pitch between 20°C and 40°C can also be crudely estimated from the two curves in Fig. 5-1.[35] The actual samples used to observe the various

phase-matched mode combinations are listed in Table 5-1.

Samples were prepared by placing a few drops of the thoroughly mixed (in the isotropic liquid phase) mixture within a ring of teflon or mylar on a glass window. A second window was then pressed upon the first and the two were held together in a simple press. Samples up to ~250 μm in thickness were obtained which were clear and uniform to the naked eye. Under a polarizing microscope however small regions were discernable with slightly different optical properties, indicating slightly different alignments of the helical structure within the domains. The effects on phase-matched third-harmonic generation of a distribution of helical-axis alignment is discussed in Section VI. Most of our experiments were done with 130 μm thick samples. Samples with relatively random and mixed helical-axis orientations (desirable for some pitch-measuring techniques) were obtained by increasing the thickness or by subjecting samples to thermal shocks such as quick melting and cooling.

Prediction of the precise pitches for phase matching reauires the measurement of ε and α (Eqs. (4-11), (3-10), and (3-12) through (3-15)). ε (Eq. (3-14) is the average dielectric constant over the two principle axes ξ and η. We measured $\varepsilon(\omega)$ in the isotropic liquid phase where the relatively random orientations of the molecules gives the desired average. We used the prism method[36] with a mercury-arc lamp as the light source and a filtered photomultiplier tube as the detector. The results the ε at the laser frequency (λ_ω = 1.06 μm) and its third harmonic ($\lambda_{3\omega}$ = 1.06 μm) are given in Table 5-1. By using ε as measured in the isotropic liquid phase as the appropriate ε for the liquid-crystal phase we are neglecting its temperature and phase -ependence. These are reasonable approximations in light of the small temperature difference between the temperatures at which ε was measured and the temperatures for phase matching (typically ~25°C) and the small difference in molecular

interaction between the two phases.

The parameter α (Eq. 3-15) is proportional to the birefringence in the twisted frame. It is most easily obtained from Eq. (3-28) by measuring the optical activity of the sample. In the region of applicability (see Fig. 3-4) α^2 is given by

$$\alpha^2 = \left|\frac{4}{\pi} p\lambda'^2(1-\lambda'^2)\, R\right| \quad , \tag{5-1}$$

where R is the optical rotation per unit length. We measured the optical activity at the He-Ne laser frequency (6328 Å) and we assume that the dispersion of α is negligible. For all sample mixtures α showed a temperature dependence, decreasing with increasing temperature.[37,38] In Table 5-1 we list our measured valves of α at the temperatures corresponding to the pitches for phase matching for the various sample mixtures. The optical activity of the 0% cholesteryl chloride mixture was unobservably small at λ_o = 6328 Å and p = 0.24 μm (the phase-matched pitch observed with this mixture). Eq. (3-28) shows that optical rotation decreases sharply with decreasing p, and should be only ~ 0.5 degree/25 μm under the above conditions. However to within our experimental uncertainty the $\alpha(T)$ curves for all the other mixtures in this three-component series were identical over the regions of interest for phase-matched third-harmonic generation. Hence we assumed the value of α for the 0% cholesteryl chloride mixture to be that of the other mixtures at equivalent temperatures, namely 0.027.

From the values of ε and α in Table 5-1 and using Eqs. (4-11), (3-10), and (3-12) through (3-15), one can calculate the predicted

pitches for phase matching with the various mode combinations. These pitches are given in Table 5-2.

We used three experimental techniques for measuring the actual pitches of our samples. For pitches significantly greater than optical wavelengths two techniques are convenient. Direct observation in a polarizing microscope can reveal the periodic structure as alternating light and dark bands,[39] whose periodicity is p/2. This method requires knowing the orientation of the helical axis in the region being examined, and the axis must have a component perpendicular to the microscope axis. A generally more convenient technique is the diffraction method.[26] If a sample has a uniformly oriented helical-axis aligned parallel to the glass windows, a laser beam propagating normal to the sample and polarized normal to the helical axis will generate diffraction spots at angles θ (with respect to the sample normal or beam direction) satisfying

$$\sin\theta = \frac{N\lambda_o}{p/2} \tag{5-2}$$

where N is an integer and $\lambda_o = 2\pi\frac{\omega}{c}$. If the laser is polarized parallel to the helical axis no diffraction pattern appears; in this case the dielectric response of the medium is not periodic since the polarization is perpendicular to the long axis of all molecules in the structure. If the sample region probed by the beam has sufficiently random orientation of the helical axis, diffraction will yield arcs or rings satisfying the same relation (Eq. (5-2)).

For pitches in the vicinity of the visible spectrum the pitch may be deduced from measurements of reflectivity or transmisivity as a function of wavelength. At the center of the reflection band, $\lambda' = 1$, or $p = \lambda/\sqrt{\varepsilon(\lambda)}$. Thus measurement of the center of the reflection band and $\varepsilon(\lambda)$ gives the pitch. The center of the reflection band is most easily measured in thin ($\lesssim 10$ μm) samples, in which the band has a true peak; in thicker samples the finite region of total reflectivity of mode 1 makes the center of the band more difficult to determine.

In the regions where these three techniques for measuring pitch overlap they are in good agreement.

In Table 5-2 we list the temperatures at which the various experimental mixtures have the pitches predicted for phase-matching, together with the accumulated uncertainty in these predictions. Most of the uncertainty arises from the measurement of $\varepsilon(\omega)$, which enters the theoretical expressions both explicitly and indirectly through our experimental determinations of α and p. Table 5-2 also lists the rate of change of pitch with temperature in the same regions.

Each of the listed phase-matched mode combinations may of course be observed in cholesteric media of either sense - right- or left-handed. The only difference is the senses of polarization of the normal modes and hence the senses of incident-light polarization necessary to excite efficiently the desired modes. The sense of the twist of a cholesteric material may be determined either from the direction of its optical rotation (see Eq. (3-28) and Fig. 3-4) or from the polarization of the reflected light at $\lambda' = 1$. In the reflection band one circularly polarized component of the incident light is strongly reflected and the other is virtually all transmitted (Figs. 3-5

and 3-6). The sense of the twist is the same as the sense of polarization[29] of the strongly reflected light at $\lambda' = 1$. The cholesteric mixture we used to observe the fourth mode combination had a left-handed structure at the lower temperature and a right-handed structure at the higher temperature (Table 5-1). All the other mixtures had left-handed structures, as indicated by the negative signs of the predicted pitches in Table 5-2.

We used a mode-locked Nd:glass laser as the fundamental pump field. A typical pulse train lasted about 200 ns with the individual pulses separated by about 7 ns. The total energy in each train was about 0.03 joule and the typical average individual pulse width was about 6 ps (as measured by two-photon fluoresence[40,41] and third harmonic generation[33]). The beam diameter was ~ 2 mm.

The experimental arrangement for measuring the phase-matched third-harmonic involving a single propagation direction for the fundamental waves (mode combinations #'s 4, 10 and 14 in Table 5-1) is shown in Fig. 5-2. The laser beam was always circularly polarized, first, because the two circular polarizations are nearly the optimum polarizations for exciting the two normal modes (see Fig. 3-5) in all the samples of interest to us, and second because this eliminated the background third harmonic radiation generated from the cell windows, optical filters and the water bath, since no third harmonic can be generated in an isotropic medium by a circularly polarized beam.[42] The third-harmonic blocking filters are necessary to eliminate the third harmonic generated in the laser cavity. The samples were immersed in a water bath with the temperature controlled to within ± 0.02°C. Typically the temperature was swept very slowly (0.1 to

0.01 °C/min) through the region of a predicted third-harmonic peak, while the third harmonic signal was measured every 2 or 3 minutes A 1P21 photomultiplier tube detected the signal, which was normalized against the reference signal of third harmonic generated in a phase-matched solution of fuchsin basic dye dissolved in hexafluoracetone sesquihydrate.[2] The response time of the whole detection system was sufficiently long that individual pulses were averaged out. The signal was measured as the area under the oscilloscope trace for a whole pulse train.

To observe the mode combination 2,2,2 → 2 (#4 in Table 5-2) the detection apparatus was placed so as to intercept the beam propagating forwards out of the sample. The experimental results of variation of third-harmonic intensity around the phase-matching temperatures are shown in Fig. 5-3. The two peaks at $p < 0$ ($T < 51.9°C$) and at $p > 0$ ($T > 51.9°C$) correspond respectively to fundamental pump waves being right- and left-circularly polarized, as predicted by the theory. The peaks appear at temperatures within 0.1°C of the predicted phase-matching temperatures. The theoretical phase-matching curve is also shown in the figure for comparison with the experimental data. The experimental peaks are definitely broader with no clear fine structure at the wings. This is probably due to the slight variation of the helical pitch in the sample, expecially near the boundary surfaces. Since the molecular structures for $p > 0$ and $p < 0$ are different and $\underset{\approx}{\chi}^{NL}$ could vary accordingly, we would not expect the two phase-matching peaks to be of the same height. Experimentally, we found that the two peaks were different in height, but their difference was within the 20% experimental accuracy.

The third-harmonic output was found to be elliptically polarized with the ratio of the two circularly polarized components being 5 ± 1. The theoretical ratio, given by[16] $|[(\lambda' - \varepsilon^{1/2})\, f_+^{(3\omega)} - m_+^{(3\omega)}]/[(\lambda' + \varepsilon^{1/2})\, f_+^{(3\omega)} - m_+^{(3\omega)}]|^2$, is 4.8. Comparison of the phase-matched third-harmonic signals from the liquid crystal and from the fuchsin basic dye solution yields $I_{LQ}^{(3\omega)} / I_{Dye}^{(3\omega)} \sim 0.1$ for this mode combination. We also measured the phase-matched third-harmonic generation from samples with different thickness. The third-harmonic intensities were indeed roughly proportional to the square of the sample thickness.

To observe the mode combinations 1,1,1 → $\bar{1}$ and 1,1,1 → $\bar{2}$ (#'s 10 and 14 in Table 5-2) a glass-slide beam splitter was placed on the laser side of the sample to couple out some of the backward third-harmonic signal. The detector was moved to intercept this beam and a focusing lens was inserted, all as indicated in Fig. 5-2. The laser beam was left-circularly polarized to feed efficiently into mode 1 in these left-handed cholesteric structures. The experimental results of the variation of the third-harmonic power around the predicted phase-matching temperatures are shown in Figs. 5-4 and 5-5. There indeed exist peaks at the predicted phase-matching temperatures. However, the widths of the peaks are several times broader than those of the theoretical phase-matching curves for a monochromatic input laser beam. This broadening is due mainly to the large spectral content of the laser, as will be discussed later. As a further confirmation of the theoretical predictions, we found in the same temperature ranges no phase-matching peak for third-harmonic generation in the forward direction and no peak for backward third-harmonic generation with the fundamental right-circularly polarized. We also found that

the phase-matched third-harmonic output was nearly left-(right-) circularly polarized for mode combination #10 (#14), as predicted by the theory. The intensities of the third harmonic generated by these mode combinations compared to that of mode combination #4 are $I^{(3\omega)}(\#10)/I^{(3\omega)}(\#4) \sim 10^{-4}$ and $I^{(3\omega)}(\#14)/I^{(3\omega)}(\#4) \sim 2 \times 10^{-14}$ (corrected for the different experimental arrangements).

The remaining mode combinations in Table 5-2 require the simultaneous presence of fundamental waves propagating in opposite directions along the helical axis. This was accomplished in two ways. One method was to construct the sample cell with a front-surface mirror in contact with the back of the sample. The mirror reflects each mode-locked pico-second pulse back on itself in the sample. Alternatively, we put a movable reflector an optical distance beyond the sample equal to the optical length of the laser cavity (Fig 5-6). This mirror directs each pico-second pulse back through the sample where it meets the next pulse in the mode-locked train passing through in the forward direction. A variable-retardation plate (stressed fused silica) in the region beyond the sample can then be used to control the polarization of the returning beam.

We observed mode combination #5$(2,2,\bar{1} \rightarrow 1)$in a cell with a reflecting back. Normally incident right-circularly polarized fundamental fed efficiently into mode #2. Upon reflection off of the mirror in contact with the back of the sample, the sense of circular polarization is reversed, becoming left handed; hence mode 1 propagating backwards is excited. The third harmonic generated in the forward direction is also reflected by the same mirror and emerges from the sample propagating backwards. Again a glass-slide beam splitter

couples out some of the third harmonic signal. The experimental results (Fig. 5-7) show a peak at the predicted temperature. The width is again due primarily to the spectral content of the laser. Relative intensity measurements give $I^{(3\omega)}(\#5)/I^{(3\omega)}(\#4) \sim 4 \times 10^{-4}$.

The same experimental arrangement gave the results shown in Fig. 5-8 for the 22% cholesteryl chloride mixture around the predicted phase-matching temperatures of mode combinations #'s 11, 12 and 13. All three of these mode combinations are predicted to be phase matched at the same pitch (352 nm). However the peak in Fig. 5-8 is due only to mode combination #13 $(1,1,\bar{2} \rightarrow \bar{2})$ because of the particular fundamental wave polarizations in the medium resulting from circularly polarized incident laser light. Relative intensity measurements give $I^{(3\omega)}(\#\ 13)/I^{(3\omega)}(\#4) \sim 10^{-2}$, and again the width of the peak is due to the broad spectral content of the laser.

This same cholesteric mixture (22% cholesteryl chloride) was also studied in an ordinary transparent cell using the experimental arrangement shown in Fig 5-6. With no retardation plate in front of the mirror, we have the same relation between the two fundamental beam polarizations as in the previous case with the mirror in contact with the sample. A left-circularly polarized incident laser beam excites mode 1. Upon reflection at the mirror the polarization is reversed to right circular, which then on passing back through the sample will excite mode 2 propagating backwards, i.e., mode $\bar{2}$. Hence only mode combination # 13 can generate third harmonic and the signal should emerge propagating backwards and be right-circularly polarized. Experimentally we found the ratio of right- to left-circularly

polarized third harmonic propagating backwards to be ~ 10/1 and found no third harmonic generated in the forward direction. We also verified the necessity for the simultaneous presence of laser light propagating both forwards and backwards in order to generate phase-matched third harmonic via this mode combination (# 13). The width of the mode-locked laser pulses was ~ 6 ps, corresponding to ~ 1 mm inside the sample. By translating the movable mirror over distances of ~ 1 mm forward or backward from the position yielding the maximum signal, we essentially eliminated the third-harmonic signal, thus confirming the requirement of opposed beams. Conversely, such observations are in fact a measure of the pulse width (Section VI).

Inserting a 1/4 λ retardation plate (at 1.06 μm) in front of the mirror (Fig. 5-6) results in the backward propagating fundamental wave in the sample having the same sense of circular polarization as the forward wave. This should excite only mode combination # 11, and indeed, we found the third harmonic to be nearly left-circularly polarized in this case, as predicted by the theory. Relative measurements give $I^{(3\omega)}(\#\ 11)/I^{(3\omega)}(\#4) \sim 3 \times 10^{-3}$.

Excitation of mode combination # 12 requires both left and right circularly polarized laser light propagating in one direction. Experimentally this is easily achieved by using linearly polarized incident light. But then a relatively large background signal is created by third harmonic generation in the cell windows, water bath and other optical components. This problem plus a weak signal to begin with made it impossible for us to make any good measurements of mode combination # 12. (The expected (see Section VI) intensity of this peak compared to that from mode combination # 4 is $\sim 3 \times 10^{-3}$;

the relative background signal with <u>linearly</u> polarized laser light is $\sim 2 \times 10^{-2}$.)

The final group of mode combinations, #'s 6, 7, 8 and 9 also have very closely grouped pitches for phase matching. With the 40% cholesteryl chloride mixture in a cell with a reflecting back we obtained the results shown in Fig. 5-9. The small peak at 31.2°C comes from mode combination #6, as predicted by the theory. The other three mode combinations are predicted to be phase matched all at essentially the same temperature, 30.1°C, and there is a strong peak at this temperature. However, similarly to previously discussed cases, the fundamental wave with right-circular polarization in this experimental arrangement selectively excites mode combination # 9. Relative intensity measurements give $I^{(3\omega)}(\#9)/I^{(3\omega)}(\#4) \sim 3 \times 10^{-1}$.

We studied this same cholesteric mixture in an ordinary transparent cell in the experimental arrangement shown in Fig. 5-6. Again with no retardation plate in front of the mirror, only mode combination #9 was excited. Experimentally the third harmonic signal was propagating in the same direction as the right-circularly-polarized fundamental beam and had a 30/1 ratio of right- to left-circularly polarized components. Inserting a quarter-wave plate for λ = 1.06 μm in front of the mirror and using right-circularly-polarized incident laser light should exclusively excite mode combination #8. Experimentally we found only 1/3 of the third harmonic to have the appropriate polarization (left-circular) for mode 1. Presumably our fundamental polarizations were not perfect and a small amount of third harmonic from mode combination #9 obscured signal from #8. We estimate $I^{(3\omega)}(\#8)/I^{(3\omega)}(\#4) \lesssim 2 \times 10^{-2}$. No observations of mode combination #7 were made, again because of the large background third

harmonic resulting from the necessity of using linearly polarized fundamental light to observe this mode combination.

In principle, second-harmonic generation can also be phase matched in a cholesteric liquid crystal. The mode combination 2, 2 → 2 is phase-matched for second-harmonic generation for p ≃ 28 μm in the same mixture we used to observe phase-matched third-harmonic generation via mode combination 2, 2, 2 → 2 (#4). However we observed no peak in second harmonic generation around this pitch. This is presumably because the overall molecular arrangement in planes perpendicular to the helical axis has an inversion symmetry. Durand and Lee[11] and Goldberg and Schnur[12,13] have also found the absence of second-harmonic generation in liquid crystals and have come to the same conclusion.

Table 5-1. Empirical data on cholesteric mixtures used to observe phase-matched third-harmonic generation. The bars over the mode numbers designate the same mode propagating in the opposite ($-\hat{z}$) direction (i.e., with a negative pointing vector).

Table 5-1

Mode Combination	Approximate Pitch For Phase Matching (μm)	% Cholesteryl Chloride In Sample Mixture[a]	Dielectric Constant[c] ε(1.06μm) ± 0.01	Dielectric Constant[c] ε(0.353μm) ± 0.01	Birefringence α At Pitch For Phase Matching ± 0.002
4. $\overbrace{2,2,2}^{\omega} \rightarrow \overbrace{2}^{3\omega}$	17	(b)	2.19	2.30	0.029[d] / 0.027
5. $2,2,\bar{1} \rightarrow 1$	1.4	48	2.20	2.32	0.030
6. $1,1,\bar{2} \rightarrow \bar{1}$	0.70				
7. $1,\bar{1},2 \rightarrow 1$	0.69				
8. $2,\bar{2},2 \rightarrow 1$	0.69	40	2.19	2.31	0.030
9. $2,2,\bar{1} \rightarrow 2$	0.69				
10. $1,1,1 \rightarrow \bar{1}$	0.47	30	2.18	2.30	0.027
11. $1,\bar{1},1 \rightarrow \bar{1}$	0.35				
12. $2,\bar{2},1 \rightarrow \bar{1}$	0.35	22	2.18	2.29	0.028
13. $1,1,\bar{2} \rightarrow \bar{2}$	0.35				
14. $1,1,1 \rightarrow \bar{2}$	0.24	0	2.17	2.27	0.027

(a) % (by weight) of cholesteryl chloride with equal parts cholesteryl oleyl carbonate and cholesteryl nonanoate.

(b) For this mode combination, samples contained 63.7% cholesteryl chloride and 36.3% cholesteryl myristate.

(c) Measured in the isotropic liquid phase at 80°C for the mixture in note (b) and at 55°C for all others.

(d) α = 0.29 for p = 17 μm and α = 0.27 for p = + 17 μm.

Table 5-2. Predicted pitches and corresponding temperatures for phase matching, and the observed temperatures and relative peak intensities of the third-harmonic peaks. dp/dT is the rate of change of pitch with temperature at the phase-matching temperatures. We use a negative pitch to indicate a left-handed cholesteric structure.

Table 5-2

Mode Combination	% Cholesteryl Chloride In Sample Mixture (a)	Predicted Pitch For Phase Matching	$\frac{dp}{dT}$ $\left(\frac{nm}{^oC}\right)$	Predicted Temperature For Phase Matching (^oC)	Observed Temperature For Phase Matching (^oC)	Relative Observed Peak Third-Harmonic Intensity
4. $\overbrace{2,2,2}^{\omega} \rightarrow \overbrace{2}^{3\omega}$	(a)	- 17.3 ± 1 μm	6400	49.4 ± 0.2	49.3	1
		+ 17.5 ± 1 μm	6400	54.2 ± 0.2	54.1	1
5. $2,2,\bar{1} \rightarrow 1$	48	-1377 ± 10 nm	39	33.3 ± 0.3	33.6	4×10^{-4}
6. $1,1,\bar{2} \rightarrow \bar{1}$		-700 ± 5 nm	8.5	31.1 ± 0.6	31.2	$\leq 3 \times 10^{-2}$
7. $1,1,\bar{2} \rightarrow 1$	40	-689 ± 5 nm	8.5	30.1 ± 0.6		
8. $2,\bar{2},2 \rightarrow 1$		-689 ± 5 nm	8.5	30.1 ± 0.6		$\leq 1 \times 10^{-2}$
9. $2,2,\bar{1} \rightarrow 2$		-687 ± 5 nm	8.5	30.0 ± 0.6	29.9	3×10^{-1}
10. $1,1,1 \rightarrow \bar{1}$	30	-472 ± 3 nm	3.6	38.2 ± 1	38.1	1×10^{-4}
11. $1,\bar{1},1 \rightarrow \bar{1}$		-352 ± 2 nm	1.3	32 ± 2		3×10^{-3}
12. $2,\bar{2},1 \rightarrow \bar{1}$	22	-352 ± 2 nm	1.3	32 ± 2		
13. $1,1,\bar{2} \rightarrow \bar{2}$		-352 ± 2 nm	1.3	32 ± 2	30.5	1×10^{-2}
14. $1,1,1 \rightarrow \bar{2}$	0	-237 ± 2 nm	0.7	38 ± 3	29.5	2×10^{-4}

(a) See notes for Table 5-1.

Chapter V Figure Captions

Fig. 5-1. Center of the reflection band at two temperatures as a function of the percentage of cholesteryl chloride in a mixture containing equal amounts of cholesteryl oleyl carbonate and cholesteryl nonanoate (all by weight). The reflected color is expressed as the inverse of its wavelength in air, which is equal to $(p\sqrt{\epsilon})^{-1}$ where p is the pitch of the cholesteric structure and ϵ is its average dielectric constant (Eq. (3-14)) at the frequency of the reflected light. A negative (positive) sign indicates a left-(right-) handed cholesteric structure. Mixtures containing $\gtrsim$ 80% cholesteryl chloride are relatively unstable at temperatures lower than the true solid-crystal to liquid-crystal transition temperature (~ 95°C for pure cholesteryl chloride). They are "super-cooled" liquid-crystal mixtures and are unstable to the onset of solid crystallization; when freshly prepared and cooled from the liquid phase to around room temperature, these high cholesteryl-chloride-content liquid-crystal structures last on the order of minutes before making the transitions to the ordinary solid crystal phase.

Fig. 5-2. Experimental arrangement for observing third-harmonic generation in temperature-tuned cholesteric liquid crystals. Numbers refer to Corning and Scholt glass filters. The main laser beam passes through a linear polarizer (Lp), a glass-slide beam splitter (Gs) and a 1/4 wave plate ($\frac{1}{4}\lambda$) for 1.06 μm. Glass filters then absorb any third harmonic generated up to this point before the beam enters the liquid crystal sample (LQ) immersed in a temperature-controlled water bath (WB). An aqueous

solution of $CuSO_4$ then filters out the laser light before the third-harmonic signal passes through an interference filter (IF) and the detector, a 1p21 photomultiplier tube. The reference arm (for normalization) generates third harmonic in a cell containing a solution of fuchsin basic (FB) in hexafluroacetone sesquihydrate. Laser attenuation filters (LF) and a 15 cm focal-length lens (L) could be inserted. The second glass-slide beam splitter and alternate detector position were used for observing third-harmonic signal generated in the backward direction.

Fig. 5-3. Normalized third-harmonic intensity versus temperature near the phase-matching temperatures for the mixture of 1.75: 1.00 by weight of cholesteryl chloride and cholesteryl myristate, in a cell 130 μm thick. The peak at the lower temperature (corresponding to left helical structure) is generated by right-circularly polarized fundamental waves and the one at the higher temperature by left-circularly polarized fundamental waves. The solid line is the theoretical phase-matching curve and the dots are experimental data points. The uncertainty in the experimental third-harmonic intensity is about 20%.

Fig. 5-4. Normalized third-harmonic power generated in the backward direction as a function of temperature in a mixture of 35:35:30 by weight of cholesteryl oleyl carbonate, cholesteryl nonanoate, and cholesteryl chloride, in a cell 130 μm thick. The phase-matching peak appears at the predicted temperature of 38.2 ± 1°C for mode combination #10. The circles are the experimental data and have about a 20% uncertainty. The solid line is a

theoretical phase-matching curve, assuming the laser pulses had a spectral content of 150 Å.

Fig. 5-5. Normalized third-harmonic power generated in the backward direction for a mixture of 50:50 by weight of cholesteryl oleyl carbonate and cholesteryl nonanoate, in a cell 130 μm thick. The peak occurs within the uncertainty of the predicted temperature (38 ± 3°C) for mode combination #14. The circles are experimental points with an uncertainty of 20%. The curve is a smooth fit to the data.

Fig. 5-6. Experimental arrangement for observing phase-matched third-matched third-harmonic generation in liquid crystals requiring the simultaneous presense of laser light propagating both forwards and backwards. The two optical path lengths marked "L" in the figure must be equal to ensure the coincidence of the pico-second mode-locked pulses in the sample, since their separation as they come out of the laser is the round-trip transit-time in the laser cavity. The unlabled optical components are the same as in Fig. 5-2. The glass-slide beam splitters (GS) for coupling out the third-harmonic signal were oriented as close (~ 10°) as practicable to perpendicular to the laser beam so as to minimize the change of polarization of the reflected third-harmonic signal as well as the transmitted fundamental beams. An adjustable retardation plate (RP) stands in front of a movable mirror MM. The reference third-harmonic apparatus (REF) is the same as in Fig. 5-2.

Fig. 5-7. Normalized third-harmonic power around the predicted phase-matching temperature for mode combination #5 (33.3 ± 0.3°C),

for a mixture of 26:26:48 by weight of cholesteryl oleyl carbonate, cholesteryl nonanoate and cholesteryl chloride, in a cell 130 μm thick with a reflecting back. The circles are experimental points with an uncertainty of 20%. The curve is a smooth fit to the data.

Fig. 5-8. Normalized third-harmonic power around the predicted phase-matching temperature for mode combinations #'s 11, 12 and 13, for a mixture of 39:39:22 by weight of cholesteryl oleyl carbonate, cholesteryl nonanoate and cholesteryl chloride, in a cell 130 μm thick with a reflecting back. The circles are experimental points with an uncertainty of about 20%. The curved is a smooth fit to the data.

Fig. 5-9. Normalized third-harmonic power around the predicted phase-matching temperatures (32±2°C) for mode combinations #'s 6, 7, 8 and 9, for a mixture of 30:30:40 by weight of cholesteryl oleyl carbonate, cholesteryl nonanoate, and cholesteryl chloride in a cell 130 μm thick with a reflecting back. The circles are experimental points with an uncertainty of 20%. The curve is a smooth fit to the data.

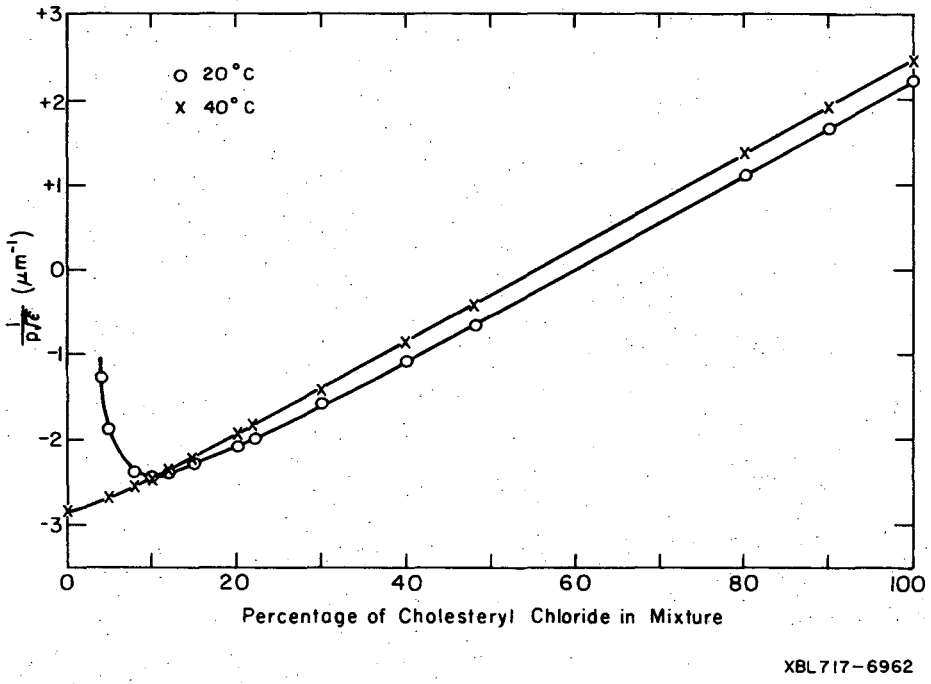
o 20°c
x 40°c
+3
+2
+1
0
-1
-2
-3
0
20
40
60
80
100
Percentage of Cholesteryl Chloride in Mixture
XBL717-6962

Fig. 5-1

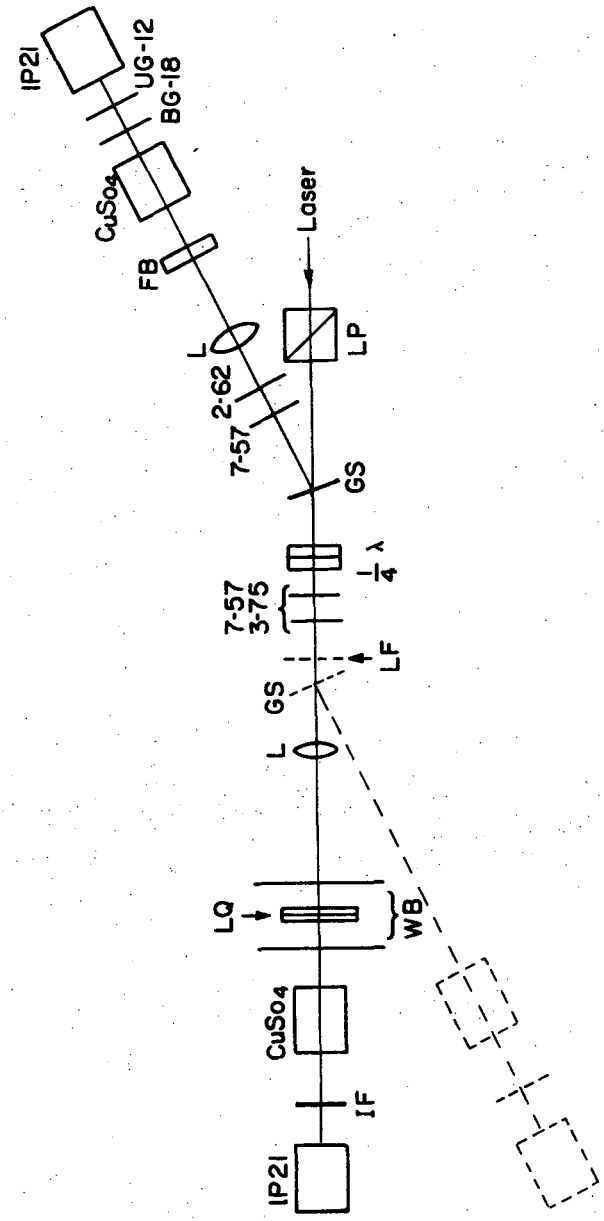
IP21
UG-12
BG-18
CuSo4
FB
L
2-62
7-57
GS
Laser
LP
1/4 λ
7-57
3-75
LF
GS
L
LQ
WB
CuSo4
IF
IP21
XBL717-6963

Fig. 5-2

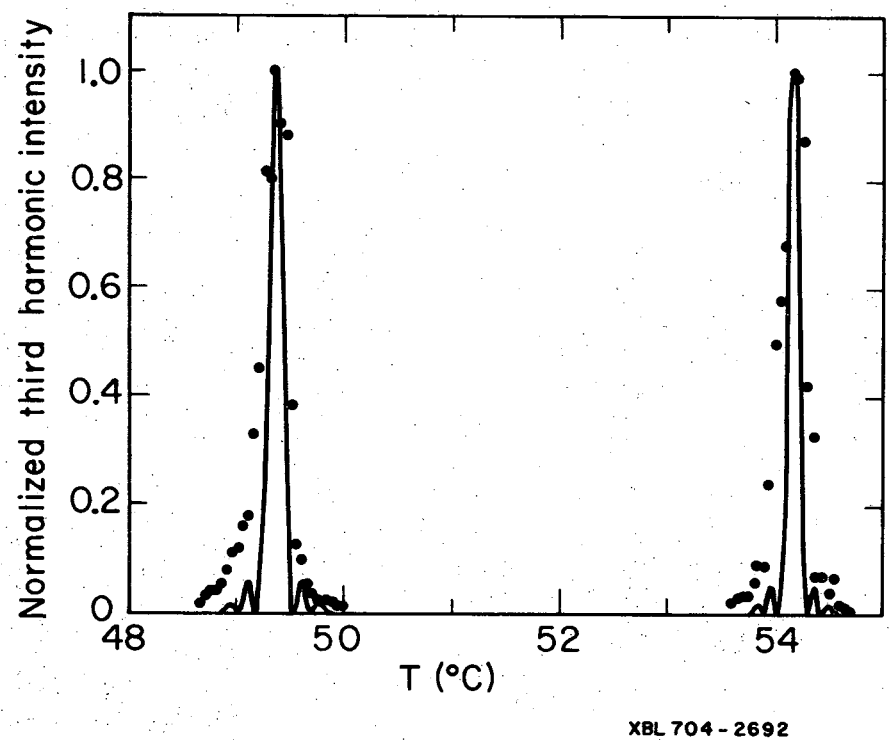
Normalized third harmonic intensity
1.0
0.8
0.6
0.4
0.2
0
48
50
52
54
T (°C)
XBL 704-2692

Fig. 5-3

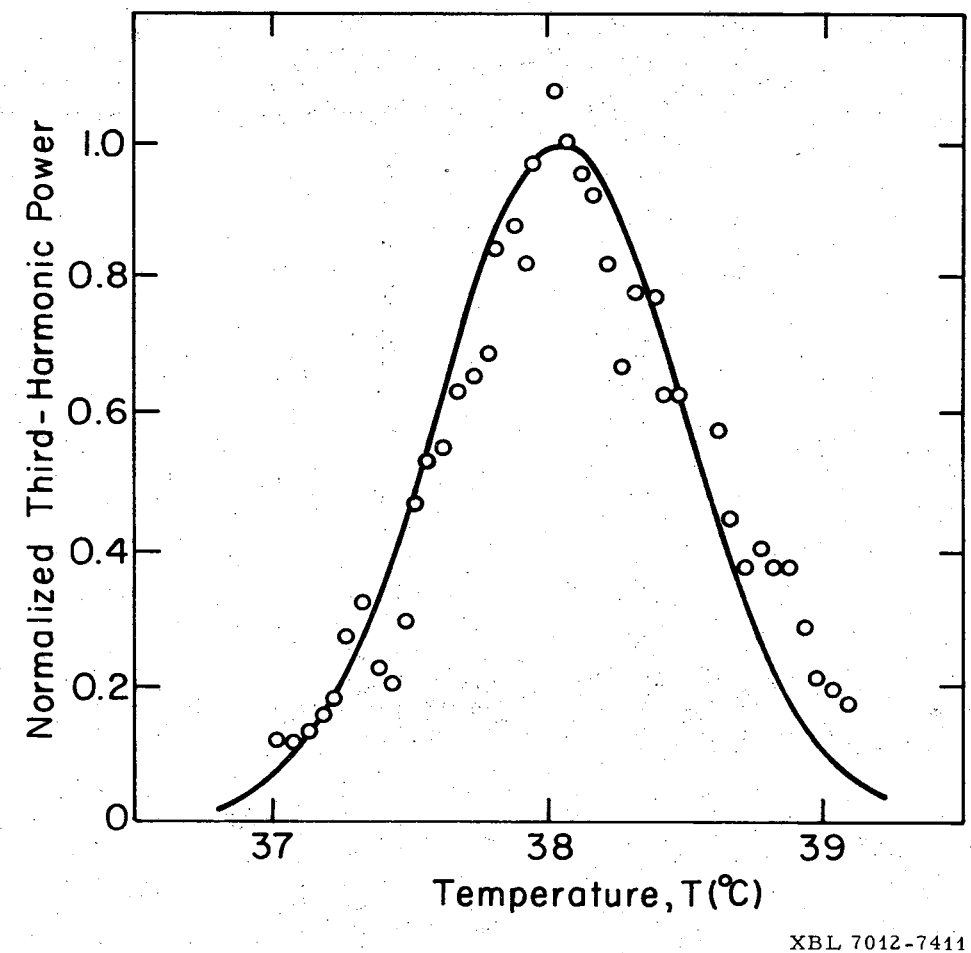
Normalized Third-Harmonic Power
1.0
0.8
0.6
0.4
0.2
0
37
38
39
Temperature, T(°C)
XBL 7012-7411

Fig. 5-4

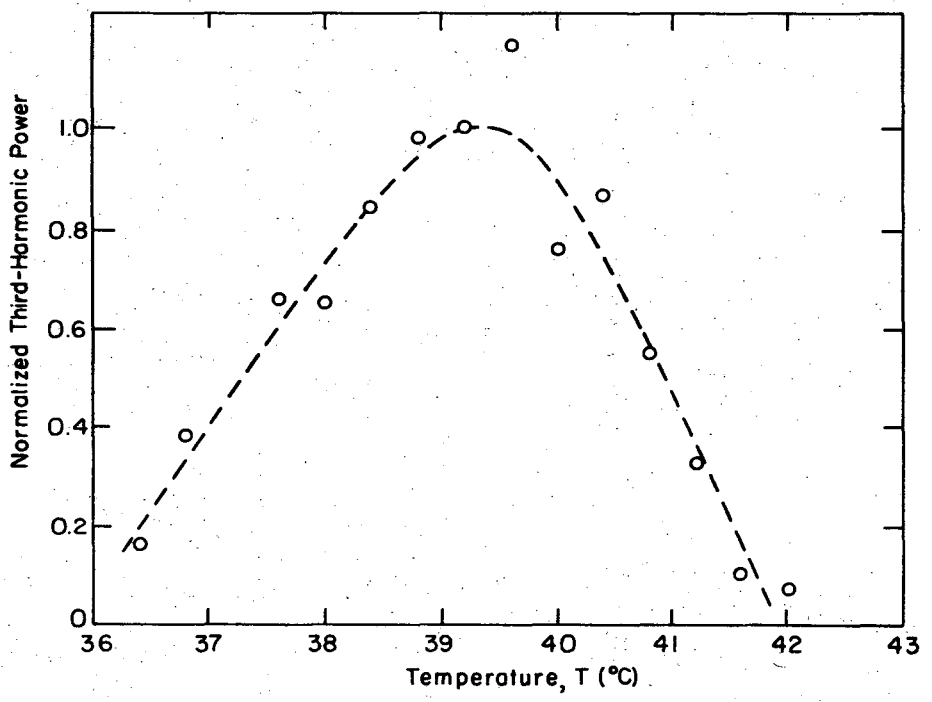

XBL 717-6964

Fig. 5-5

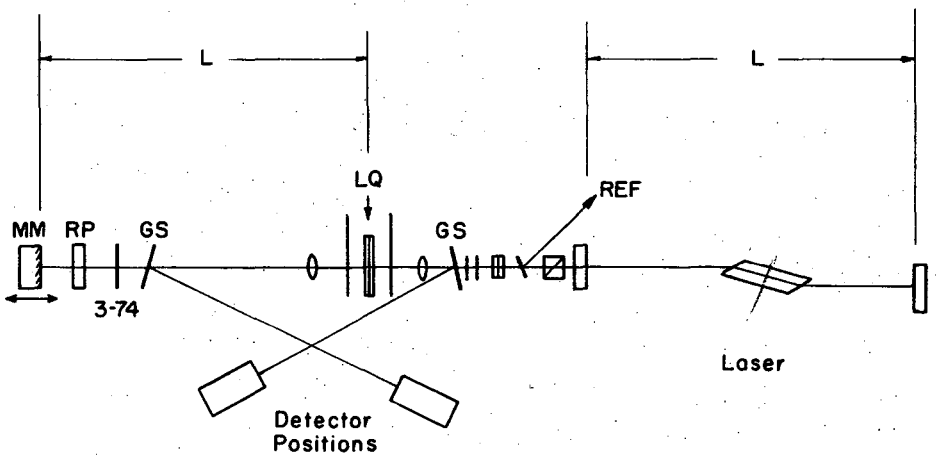

XBL 717-6965

Fig. 5-6

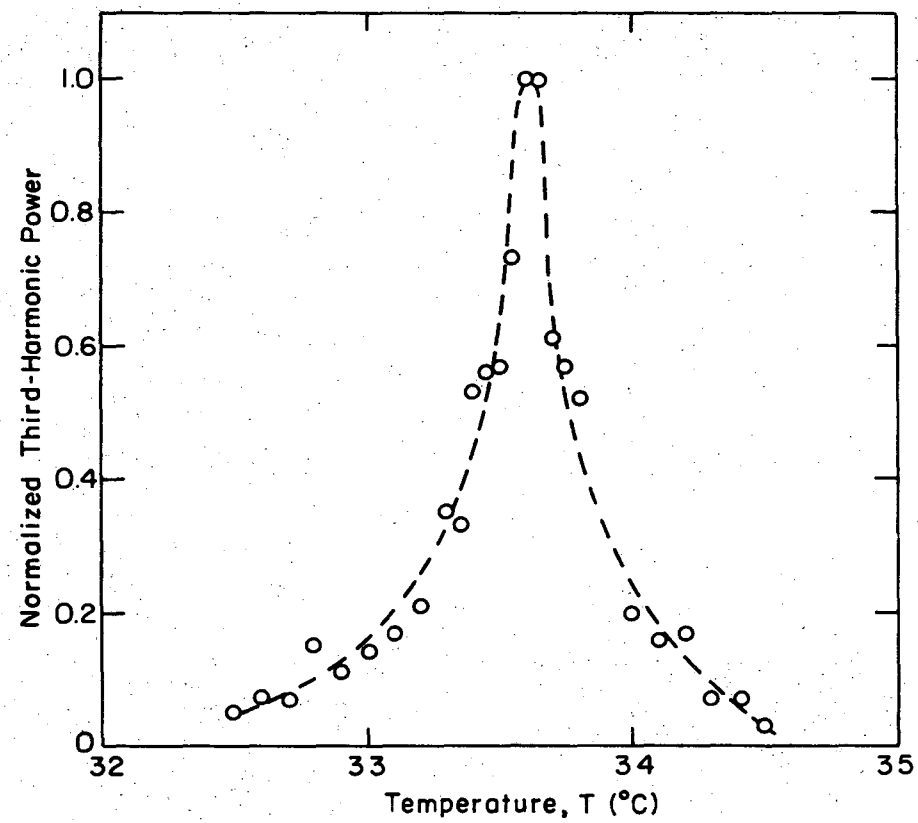

XBL717-6966

Fig. 5-7

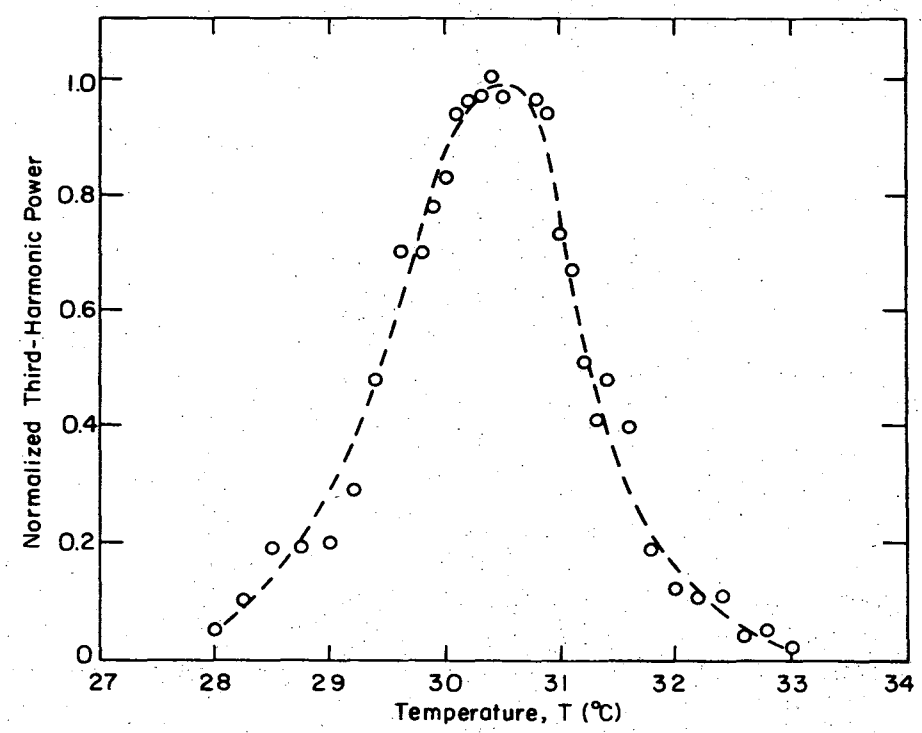

XBL717-6967

Fig. 5-8

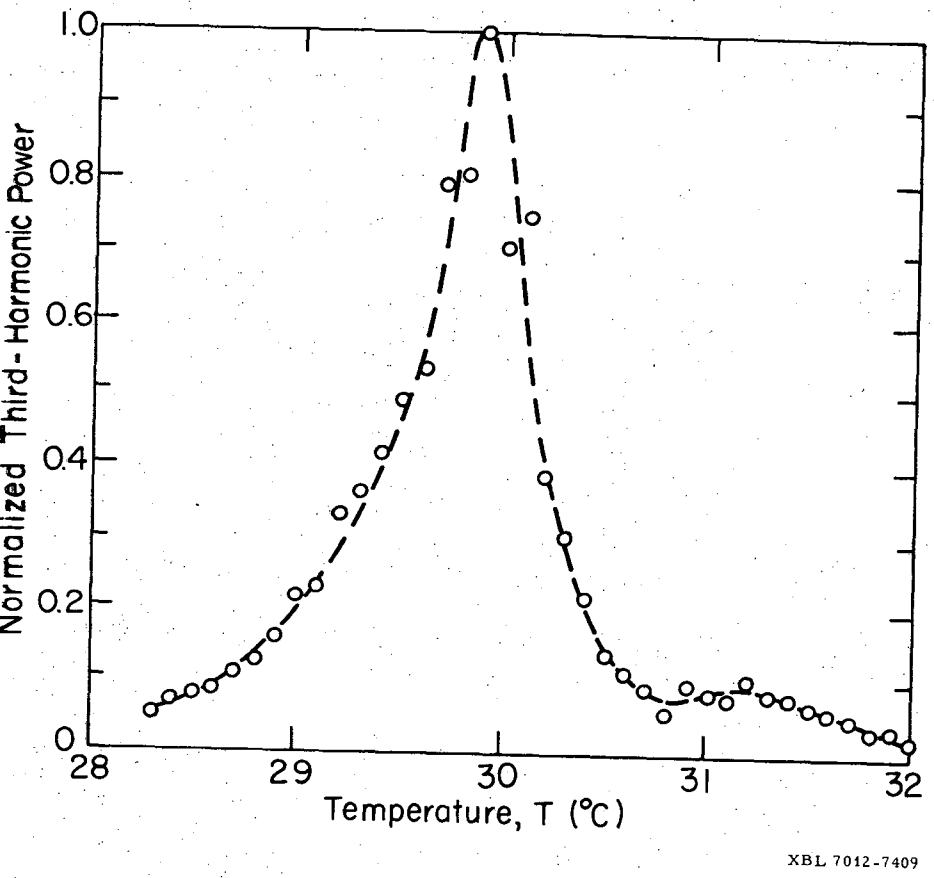

Fig. 5-9

VI. DISCUSSION AND CONCLUSIONS

In all cases, the widths of our observed phase-matching peaks (as a function of temperature or pitch) are greater than predicted theoretically for a monochromatic laser and a perfect liquid-crystal sample. If the laser beam were monochromatic and the liquid crystal were as idealized in our theory, the widths of the phase-matching curves would depend on the rate of change of the index mismatch Δk (Eq. (4-11)) with pitch and the thickness of the sample. The full width at half maximum would be given by

$$(\Delta p)_1 = \frac{\pi}{L \frac{d(\Delta k)}{dp}} \tag{6-1}$$

where L is the sample thickness. The value of i.e. $(\Delta p)_1/p$ for each of the carefully observed mode combinations is given in Table 6-1.

But two other effects in fact dominate the observed widths. Many liquid-crystalline molecules exhibit strong surface effects; in many materials the initial orientation of the boundary layer of molecules appears to remain unchanged despite changes in temperature even including phase changes.[43] In a sample of cholesteric material, the molecular alignment at both interfaces may therefore be fixed. These constraints would not allow a perfect helical structure of arbitrary pitch to fit between the two interfaces. There would in general be a distortion of the helical structure amounting to ~ p/2 over the sample thickness (L). This implies a pitch distribution with a width $(\Delta p)_2 \sim \frac{1}{2} \frac{p^2}{L}$. The values of $(\Delta p)_2/p$ at the phase-matching pitches are given in Table 6-1. This effect clearly increases with pitch, and apparently is the dominant contribution in our observations of

the third-harmonic peak for $p \sim 17$ μm (mode combination #4). For this peak, $(\Delta p)_2/(dp/dt) \sim 0.2°C$, and $(\Delta p)_1/(dp/dT) \sim 0.1°C$. Our observed full width at half maximum is $\sim 0.3°C$.

For all the other phase-matched mode combinations we observed, the dominant broadening effect comes from the large spectral content of the mode-locked laser. The different frequencies within the laser's spectral width are phase matched for third-harmonic generation at different pitches. Thus as one varies the pitch (by changing the temperature) one brings different frequencies (or, more generally, frequency combinations) into a phase-matched condition for third harmonic (or, more generally, sum frequency) generation. By assuming a spectral content of the mode-locked laser pulses of about 150 Å (full width at half maximum of a Gaussian pulse) due mainly to frequency chirping, we obtain a contribution to the widths $(\Delta p)_3/p = 7.5 \times 10^{-3}$ at any pitch and for all mode combinations, as indicated in Table 6-1. This is clearly the dominant contribution for all the other observed peaks and gives good agreement with the observed widths (Table 6-1).

Observations of our samples under a polarizing microscope and of the angular distribution of reflected light from a resonant ($\lambda' = 1$) sample indicate the alignment of the helical axis is not uniform. However this does not affect the observed widths of our third-harmonic peaks. Phase matching is achieved in cholesteric liquid crystals through the contribution of one or more units of lattice momentum to the required overall momentum balance. The lattice momentum is always parallel to the helical axis. Our third harmonic detector was always positioned so as only to admit signal ~ co-linear with the fundamental beam(s). The momentum mis-match among co-linear optical fields is

always co-linear with their propagation direction and hence it cannot be compensated by the lattice momentum in a mis-aligned cholesteric structure. Phase matching can be achieved for off-axis beams, but only if they are non-co-linear in such a way as to conserve their components of momentum perpendicular to the helical axis, since the medium's contribution can only be parallel to the axis.

In our experimental arrangement the third-harmonic detector had an acceptance angle of ~3°; consequently, consideration of the vectors in phase matching indicates we could observe phase-matched harmonic generated from a ~3° range of domain alignments. Phase-matching occurs in a domain tipped ~ 1.5° at a pitch difference $\Delta p/p \sim 3 \times 10^{-4}$ compared to an aligned domain. This is always small compared to other effects as can be seen in Table 6-1 and thus does not contribute to our observed widths. (The laser beam convergence was $\lesssim 1°$ when focused, and so did not contribute.) There is a loss of third-harmonic power due to the fact that only the aligned (± 1.5°) regions contribute. Compared to a perfect sample, this loss is roughly proportional to the amount of misaligned (< 1.5°) sample. Rough measurements suggest an alignment distribution of ~ ± 6°. Thus our numerical estimate (below) of the C's compared to χ^{NL}_{dye} may be low by a factor of ~ 2.

From our measurements of the relative intensities of phase-matched third-harmonic generation by all these various mode combinations we are able to deduce some information about the relative values of the non-linear-susceptibility elements. Equations (4-12a) and (4-12b), and Table 4-2 give the theoretical relations between measured third-

harmonic intensities and the non-linear tensor element C_{11}, C_{12}, C_{21} and C_{22}. Making the assumption that the non-linear tensor elements are the same for all our different samples, we find that computer calculations using our relative intensity measurements of mode combinations #'s 4, 5, 9. 10, 13 and 14 corrected for their different widths indicate that all four C's are nearly equal; their values differ by from ~ 3% to ~ 10%, but the data do not justify more specific conclusions. Uncertainties in the experimental values of the parameters m', f and q in the theoretical expressions are important in some regions of pitch, but the dominant uncertainty is in our relative intensity measurements. Because of the inherently different beam geometries for the various mode combinations, the experimental arrangement could not be the same for all observations. In addition, the four orders of magnitude range in the relative third-harmonic intensities required different amounts of focusing of the laser beam(s) and attenuation of both the laser and the third harmonic. Corrections for all these different situations introduce uncertainties. Different experimental runs also yielded slightly different results, presumably due to differences in sample quality. Taken together, all these factors result in an uncertainty of about a factor of 2 in our relative intensity figures. As a consequence we can only conclude that C_{11}, C_{12}, C_{21} and C_{22} are equal to within $\lesssim$ 10% and unequal by by $\gtrsim$ 3%. Comparison with the third harmonic intensity generated in a phase-matched solution (45 gm/liter) of fuchsin dye in hexafluoracetone sesquihydrate[2] gives that the magnitude of the C's is ~ 0.2 χ^{NL}_{dye}.

In the above calculation, the experimental result for mode combination #6 was not used. Assuming the c's are equal, we compute that the expected peak from mode combination #6 should be four times greater than that from mode combination #9. Our experimental data (Fig. 5-9) indicate instead that combination #6 is only 1/10 as intense as #9, or ~ 40 times weaker than predicted. In some experimental runs no peak at all was visible at this pitch. The discrepancy between the observations and the prediction is due to strong reflection of left-circularly polarized laser light. The central laser wavelength, λ_o = 1.06 μm, is centered in the reflection band for p = 0.72 μm. Mode combination #6 is phase matched for p = 0.70 μm. The theoretical normal incidence reflectivity at 1.06 μm of a semi-infinite sample is ~ 25%. Actual measurements of the transmission in our tuned samples indicates that $\lesssim 10^{-1}$ of the left-circularly-polarized light is transmitted. In our experiments we used right-circularly-polarized incident light which was virtually all transmitted, but $\lesssim 10^{-1}$ of the reflected backward propagating left-circularly polarized light was transmitted. Since mode combination #6 involves two left-circularly-polarized fields (and one right), this effect would decrease the observed third-harmonic intensity by a factor of $\lesssim 10^{-2}$ if the left-circularly-polarized beam were weaker by 10^{-1} throughout the sample. The decrease would be somewhat less if the intensity of the left-circularly-polarized beam decreases gradually as it penetrates the sample, due

to effects not considered in our theoretical analysis (e.g., scattering losses due to imperfect cholesteric structure).

The analagous situation of high reflectivity at the third harmonic does not affect our observations. Although mode combination #14 is phase-matched for a pitch which puts the third harmonic inside its reflection band, there are no observable consequences since the harmonic is right-circularly polarized and therefore not reflected.

We note in summary that the assumption that the four non-linear tensor elements are the same for all our experimental samples is consistent (to within 10%) of our experimental results.

We also observed one of the phase-matched third-harmonic peaks in an entirely different kind of cholesteric-liquid-crystalline material. All our previously discussed observations were made using mixtures of materials all of which were chemical derivatives of the cholesterol molecule. This choice was arbitrary in some respects; any material forming a cholesteric structure with appropriate pitch and dielectric constants will generate phase-matched third harmonic. In particular, poly—γ-benzyl-L-glutamate (PBLG), a synthetic α-helix protein, dissolved in dioxane is cholesteric for concentrations from ~ 0.1 gm to ~ 0.5 gm of PBLG per gm of solvent.[19] The dielectric constants are comparable to those of our cholesterol-derived materials and hence the pitches for phase-matching are approximately the same. A pitch of ~ 17 μm is realizable and hence phase-matched third-harmonic generation via mode combination #4 should be possible. Although the pitch of PBLG in dioxane has a temperature dependence, we did not use it to tune the pitch because of the slow response time of PBLG samples under changing external conditions. (It takes weeks for a

freshly prepared sample to form a moderately uniform cholesteric structure; samples prepared from derivatives of cholesterol are usable within seconds.) Therefore we used the concentration dependence of pitch, preparing many samples with different concentrations. We observed a peak in third-harmonic intensity around p = 17 μm with the laser polarized to feed efficiently into mode #2, and no peak for the opposite laser polarization. There was a moderate amount of scatter in the data, presumably due to the use of many different samples.

We expended a good deal of effort in trying to observe phase-matched third-harmonic generation from mode combination #3 (Table 4-1). Unlike mode combinations #5 - #14, #3 is not necessarily phase-matchable at any pitch in cholesteric materials; its phase-matchability depends critically on its parameters ε and α. We believe this mode combination is phase matchable in the same cholesteric mixture we used to observed combination #4 but at a pitch $\gtrsim$ 50 μ. Our experimental efferts were largely frustrated by the poor quality of our liquid crystal samples when the pitch became this large; the samples no longer appeared clear. Others have encountered similar difficulties when the pitch approaches the sample thickness.[38,44] We did observe a slight peak at the expected pitch but could not verify the expected dependence of the peak intensity of sample thickness (square law) due perhaps, to the large light scattering in oursamples.

Recently, measurements of ultrashort pulses have attracted much attention.[40,45-47] In all cases, except the case of Treacy using the compression technique,[46] the experiments measure a correlation function which is intrinsically symmetric, so that only information about the pulse width can be obtained, and not information about the

possible assymmetry of the pulse shape. Techniques using second-harmonic generation or two-photon fluoresence measure the second order autocorrelation function, $G^{(2)}(\tau) = \int_{-\infty}^{\infty} |E(t)|^2 |E(t+\tau)|^2 \, dt$, which is inherently symmetric ($G^{(2)}(\tau) = G^{(2)}(-\tau)$). Phase-matched third-harmonic generation has been used for pulse-width measurements,[47] but under circumstances in which only a symmetrized form of the third-order autocorrelation function could be observed. Here, in principle, the technique can provide information about pulse asymmetry as well, if phase matching requires two fundamental photons in one mode and one in the other mode, since then the correlation function $G^{(3)}(\tau) = \int_{-\infty}^{\infty} |E(t)|^4 |E(t+\tau)|^2 \, dt \neq G^{(3)}(-\tau)$.[48] This is indeed the case for ~~all~~ fourteen phase matchable mode combinations except #'s 1, 4, 10 and 14. To demonstrate the technique, we split the laser beam into two beams with proper polarizations for exciting mode combination #9. The two beams, after traveling about the same optical path, met each other at t the sample from opposite sides. A variable optical delay in one arm allowed continuous variation of the relative arrival time τ of the two pulses. Our results are shown in Fig. 6-1. The curve shows an average pulse width of about 7.5 psec and a slight pulse asymmetry in the sense that the trailing edge of the pulse was steeper than the leading edge. This agrees qualitatively with the result of Treacy.[45] Assuming a hypothetical asymmetric pulse shape constructed from two half-gaussians joined at their maxima, we find a satisfactory fit to our data with the ratio of the widths of the two half-gaussians being ≥ 4. Although third order correlation functions give qualitative data about asymmetry, they are not a sensitive quantitative measure of pulse shape. Some prior knowledge of pulse shape and very precise data are necessary to draw accurate conclusions. The resolution of our data was limited by the sample thickness which was 130 μm. For better resolution and signal-to-

noise ratio, we should probably use crystals such as calcite[49] as the nonlinear medium in such measurements, where phase-matched third-harmonic generation can be achieved with two fundamental photons in the ordinary mode and one in the extraordinary mode. Since in calcite phase-matching is achieved with all fields propagating in the same direction, the resolution is not limited to the sample thickness and one can greatly increase the signal without sacrificing resolution. Ideally one might be able to obtain information about individual pulses instead of averages over all the pulses in many trains.

Our maximum observed conversion of energy from the laser frequency to the third-harmonic was small. The most efficient mode combination in this respect was #4. Without focusing the ~ 2 mm diameter laser beam, our 130 μm thick samples converted ~ 10^{-14} of the laser energy to its third harmonic. By focusing the laser beam down to ~ 0.1 mm diameter, one might increase the conversion by a factor of ~ 5×10^2. We did not observe any damage threshold; if the laser intensity did damage our samples, they recovered in the time between laser shots (~ 2 min.). We believe thicker samples are possible, but probably not without external electric or magnetic fields to maintain unfform orientation of the symmetry axis throughout the sample.[20-26,50] If the square-law dependence of third harmonic intensity on sample thickness holds up to centimeters, a 1 cm thick sample would increase the conversion efficiency by another factor of ~ 6×10^3. A laser with a peak power of ~ 10^8 watts would then generate a peak third-harmonic power of ~ 3 watts. Even this may be optimistic. It could not be achieved with a typical mode-locked Nd-glass laser because only part of its broad spectral width (~ 150 Å) can be phase-matched at a given pitch in such thick samples. In

addition even if an aligned 1 cm thick sample were achieved, imperfections could lead to dephasing and/or scattering of the beams to the extent that the square-law dependence were no longer valid. The potential of cholesteric liquid crystals as practical conversion devices thus awaits further investigation of the properties of thick ($\gtrsim$ 1 cm) samples.

We have explicitly considered the phase matching of only two interactions, second- and third-harmonic generation. In fact it is just as easy to phase match almost any other optical interaction, primarily because the periodicity of liquid crystals is continuously tunable, and it is the periodicity which gives rise to most of the phase-matching possibilities. Other large-scale-periodic media offer similar potential. Bloembergen and Sievers[51] have considered possiblities for phase matching of a number of interactions in composite layers of GaP and GaAs. This material lacks inversion symmetry, thus permitting the observation of second-order non-linear effects. However it is difficult to fabricate and not so directly tunable. The great advantage of cholesteric liquid crystals is their inherent and variable periodicity.

Table 6-1. Data on predicted and observed widths of phased-matched third-harmonic peaks in cholesteric liquid crystals. p is the approximate pitch for phase-matching of the designated mode combination; $d(\Delta k)/dp$ is the rate of change of the corresponding phase mismatch (Eq. (4-11)) with pitch and dp/dT is the rate of change of pitch with temperature around the phase-matched pitch. $(\Delta p)_1$, $(\Delta p)_2$ and $(\Delta p)_3$ are estimated contributions to the widths of the third-harmonic peaks in a sample 130 μm thick due repectively to the rate of change of the index mismatch, possible distortion of helical structure, and laser bandwidth, and are defined in the text. The total predicted width is calculated from the sum of the previous three columns, and the observed widths are given in the last column.

Table 6-1

Mode Combination	p (μm)	$\frac{d(\Delta k)}{dp}$ (μm^{-2})	$\frac{dp}{dT}$ $\frac{Å}{^oC}$	$\frac{(\Delta p)_1}{p}$	$\frac{(\Delta p)_2}{p}$	$\frac{(\Delta p)_3}{p}$	ΔT Pred. (°C)	ΔT Obs. (°C)
4. 222 → 2	17	0.04	6.4×10^4	3.3×10^{-2}	6.7×10^{-2}	7.5×10^{-3}	0.3	0.3
5. $22\bar{1} \rightarrow 1$	1.4	13	390	5.8×10^{-4}	5.3×10^{-3}	7.5×10^{-3}	0.4	0.4
9. $22\bar{1} \rightarrow 2$	0.70	27	85	1.3×10^{-3}	2.6×10^{-3}	7.5×10^{-3}	0.7	0.6
10. $111 \rightarrow \bar{1}$	0.47	110	36	4.6×10^{-4}	1.8×10^{-3}	7.5×10^{-3}	1.3	1.0
13. $11\bar{2} \rightarrow \bar{2}$	0.35	100	13	9.5×10^{-4}	1.4×10^{-3}	7.5×10^{-3}	2.2	1.7
14. $111 \rightarrow \bar{2}$	0.24	220	7	4.0×10^{-4}	9.1×10^{-4}	7.5×10^{-3}	3.0	2.8

Chapter VI Figure Captions

Fig. 6.1. Normalized third-harmonic power versus relative time delay of the two fundamental laser pulses propagating in opposite directions in the mixture of Fig. 5-9 at the phase-matching temperature 29.9°C. The circles are experimental points with an uncertainty of 20%. The dashed curve is a smooth fit to the data.

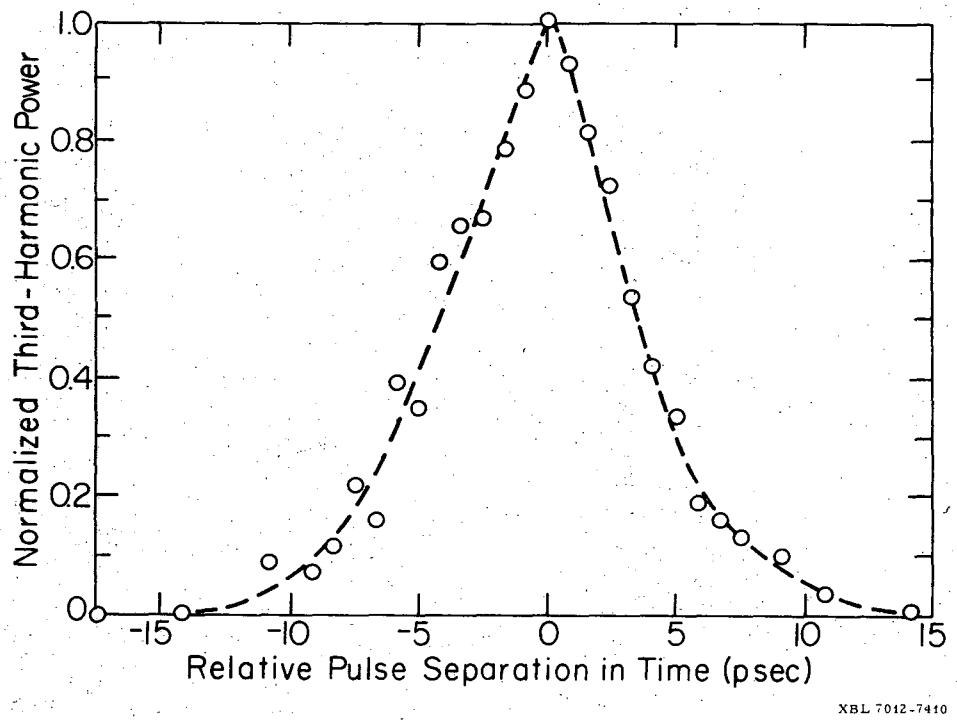

Fig. 6-1

ACKNOWLEDGMENTS

I thank Professor Y. R. Shen for his invaluable guidance and support throughout all of this project, K. Gustafson for carefully reading most of the manuscript, and N. Amer, for helping me into the beautiful and fascinating world of liquid crystals.

This work was done under the auspices of the Atomic Energy Commission.

REFERENCES

1. J. A. Armstrong, N. Bloembergen, J. Ducuing, and P. S. Pershan, Phys. Rev. 127, 1918 (1962).
2. J. P. Bey, J. F. Guiliani, and H. Rabin, Phys. Rev. Letters 19 819 (1967).
3. R. K. Chang and L. K. Galbraith, Phys. Rev. 171, 171 (1968).
4. J. A. Giodmaine, Phys. Rev. Letters 8, 19 (1962).
5. P. D. Maker, R. W. Terhune, M. Nisenoff and C. M. Savage, Phys. Rev. Letters 8, 21 (1962).
6. H. Rabin and P. P. Bey, Phys. Rev. 156, 1010 (1967).
7. C. K. N. Patel and N. van Tran, Appl. Phys. Lett. 15, 189 (1969).
8. G. W. Gray, Molecular Structure and the Properties of Liquid Crystals (Academic, New York, 1962).
9. I. G. Chistyakov, Soviet Physics Uspekhi 9, 551 (1967).
10. I. Freund and P. M. Rentzepis, Phys. Rev. Lett. 18, 393 (1967).
11. G. Durand and C. H. Lee, Molecular Crystals 5, 171 (1968).
12. L. S. Goldberg and J. S. Schnur, Appl. Phys. Lett. 14, 306 (1969).
13. L. S. Goldberg and J. S. Schnur, Radio Electronic Engr. (GB) 39, 279 (1970).
14. P. A. Franken and J. F. Ward, Rev. Mod. Phys. 35, 23 (1963).
15. C. W. Oseen, Trans. Faraday Soc. 29, 883 (1933).
16. Hn. de Vries, Acta Cryst. 14, 219 (1951).
17. J. M. Ziman, Principles of the Theory of Solids (Cambridge, London, 1964), Chpt. 1.
18. C. Kittel, Introduction to Solid State Physics (Wiley, New York, 1967), Chpt. 9..

19. C. Robinson, J. C. Ward, and R. B. Beevers, Disc. Faraday Soc. 25, 29 (1958).
20. P. G. De Gennes, Solid State Communications 6, 163 (1968).
21. R. B. Meyer, Appl. Phys. Lett. 12, 281 (1968).
22. R. B. Meyer, Appl. Phys. Lett. 14, 208 (1969).
23. F. J. Kahn, Phys. Rev. Lett. 24, 209 (1970).
24. G. Durand, L. Leger, F. Rondelez and M. Veyssie, Phys. Rev. Lett. 22, 227 (1969).
25. H. Baessler and M. M. Labes, Phys. Rev. Lett. 21, 1791 (1968).
26. E. Sackmann, S. Meiboom, L. C. Snyder, A. E. Meixner, and R. E. Dietz, J. Am. Chem. Soc. 90, 3567 (1968).
27. R. S. Porter, E. M. Barrall II, and J. F. Johnson, J. Chem. Phys. 45, 1452 (1966).
28. Hn de Vries[15] uses the oppisite sign in the exponential ($\exp(ikx + i\omega t)$), which results in some differences of sign between our formulae
29. As defined, for example, in J. D. Jackson, Classical Electrodynamics, (Wiley, New York, 1962), p. 206.
30. For a report on observations of a second-order reflection band in cholesteric materials, see D. W. Berreman and Ta. W. Scheffer, Phys. Rev. Lett. 25, 577 (1970).
31. J. M. Ziman, Electrons and Phonons (Oxford, London, 1960) p. 133.
32. M. Jean Paul Mathieu, Bull. de la Soc. Francaise de Mineralogie 61, 174 (1938).
33. J. W. Shelton and Y. R. Shen, Phys. Rev. Lett. 26, 538 (1971).
34. These chemicals were obtained from Aldrich Chemical Co., Eastman Organic Chemicals, and Varilight Corp., and were used without further purification.

35. For more information on this three-component cholesteric system see:
J. L. Fergason, Appl. Optics 7, 1729 (1968).
J. L. Fergason, Am. J. of Physics 38, 425 (1970).
L. Melamed and D. Rubin, Appl. Optics 10, 1103 (1971).

36. See, for example, F. W. Sears, Optics (Addison-Wesley, Reading, Mass., 1949), p. 47.

37. J. W. Shelton and Y. R. Shen, Phys. Rev. Lett. 25, 23 (1970).

38. H. Baessler, T. M. Laronge, and M. M. Labes, J. of Chem. Phys. 51, 3213 (1969).

39. C. Robinson, Tetrahedron 13, 219 (1961).

40. J. A. Giordmaine, P. M. Rentzepis, S. L. Shapiro and K. W. Wecht, Appl. Phys. Lett. 11, 216 (1967).

41. H. P. Weber, Phys. Lett. 27A, 321 (1968).

42. P. P. Bey and H. Rabin, Phys. Rev. 162, 794 (1967).

43. Ref. 8, p. 39; see also P. Chatelain, Bull. Soc. Franc. Mineral. Crist. 66, 105 (1943).

44. P. Kassubek and G. Meier, Mol. Cryst. and Liq. Cryst. 8, 305 (1969).

45. J. A. Armstrong, Appl. Phys. Lett. 10, 16 (1967).

46. E. B. Treacy, Appl. Phys. Lett. 14, 112 (1969).

47. R. C. Eckardt and C. H. Lee, Appl. Phys. Lett. 15, 425 (1969).

48. H. P. Weber and R. Dandliker, Phys. Lett. 28A, 77 (1968).

49. P. D. Maker and R. W. Terhune, Phys. Rev. 137, A801 (1965).

50. E. Sackmann, S. Meiboom and L. C. Snyder, J. Am. Chem. Soc. 89, 5981 (1967).

51. N. Bloembergen and A. J. Sievers, Appl. Phys. Letters 17, 483 (1970).

LEGAL NOTICE

This report was prepared as an account of work sponsored by the United States Government. Neither the United States nor the United States Atomic Energy Commission, nor any of their employees, nor any of their contractors, subcontractors, or their employees, makes any warranty, express or implied, or assumes any legal liability or responsibility for the accuracy, completeness or usefulness of any information, apparatus, product or process disclosed, or represents that its use would not infringe privately owned rights.

TECHNICAL INFORMATION DIVISION
LAWRENCE BERKELEY LABORATORY
UNIVERSITY OF CALIFORNIA
BERKELEY, CALIFORNIA 94720